ABSTRACT

Title: MODELING OF MOBILE AIR CONDITIONING SYSTEM

Zhenyuan Mei, Master of Science, 2017

Directed By: Research Professor Yunho Hwang, Ph.D.
Department of Mechanical Engineering

Since the conventional refrigerant R-134a is being phased out due to its high global warming potential, finding a suitable replacement refrigerant and a system design is of great importance. However, most of alternatives are either flammable or expensive. Therefore, to ensure the safety of passenger and reduce the refrigerant charge, a secondary loop system with coolant loop on both condenser and evaporator side was proposed. The performances of this system using R-134a, R-152a, and R-1234yf were evaluated and compared to that of conventional direct expansion system using R-134a under the US06 driving cycle condition. The results show that the coefficient of performance of the secondary loop system is significant lower than that of direct expansion system due to high pressure ratio and high compressor revolution speed. For the secondary loop system, the R-152a has better performance than R-1234yf and is a more suitable alternative refrigerant.

MODELING OF MOBILE AIR CONDITIONING SYSTEM

By

Zhenyuan Mei

Thesis submitted to the Faculty of the Graduate School of the
University of Maryland, College Park, in partial fulfillment
of the requirements for the degree of
Master of Science
2017

Advisory Committee:
Research Professor Yunho Hwang, Chair
Professor Bao Yang
Associate Professor Amir Riaz

Acknowledgements

First of all, I would like to give my sincere thanks to my advisor Dr. Yunho Hwang, who gave me continues guidance and support for my research. His insightful comments and inspiring ideas helped me a lot during these years.

Thanks to Dr. Hoesong Lee for his support at the beginning of my research. And I am also grateful for Dr. Jiazhen Ling for his guidance on transient simulation. Having a discussion with him always gave me new perspectives on problems.

Special thanks to Mr. Jae Yeon Kim for his kindness and professional opinion. And great thanks, to HYUNDAI for providing me the opportunity to develop and validate the model of mobile air conditioning system.

Last but not the least, I would like to express deepest thanks to my parents for their love and support. This work would not have been possible without them.

Table of Contents

List of Tables

List of Figures

Nomenclature

A	area [m^2]
Bo	boiling number [-]
C	refrigerant charge [kg]
c_p	specific heat capacity [$J \cdot kg^{-1} \cdot K^{-1}$]
D	diameter [m]
D_{vo}	outer volumetric diameter [m]
EM	CO_2 produced/kWh
F	Reynold number factor [-]
F_d	fin depth [m]
F_l	fin length [m]
F_p	fin pitch [m]
f	fanning friction factor [-]
H	height [m]
h	specific enthalpy [$J \cdot kg^{-1}$] or heat transfer coefficient [$W \cdot m^{-2} \cdot K^{-1}$]
h_{fg}	latent heat of vaporization per unit mass [$J \cdot kg^{-1}$]
j	Colburn j-factor [-]
L	length [m] or life time of the product [year]
L_h	lover height [m]
L_l	louver length [m]
L_p	louver pitch [m]
Le	Lewis number [-]

M	molecular weight [-]
MM	CO_2 produced/kg of material
m	mass of material
$\dot{m}$	mass flow rate [$kg \cdot s^{-1}$]
Nu	Nusselt number [-]
P	pitch [m] or perimeter [m]
p	pressure [kPa]
Pr	Prandtl number [-]
$\dot{Q}$	capacity [W]
$\dot{Q}_{plt}$	passenger latent load [W]
$\dot{Q}_{ps}$	passenger sensible load [W]
$\dot{Q}_{sol}$	solar radiation load [W]
q''	heat flux [$W \cdot m^{-2}$]
Re	Reynold number [-]
S	suppression factor [-]
T	temperature [°C]
T_d	tube depth [m]
T_p	tube pitch [m]
u	velocity [$m \cdot s^{-1}$]
V	volume [m^3]
W	width [m]
We	weber number [-]

wt.%	percentage by weight [%]
X	Martinelli number [-]
x	flow quality [-]
Δ	difference

Greek Symbols

α	dimensionless number for j-factor calculation or heat transfer coefficient [$W \cdot m^{-2}K^{-1}$]
β	dimensionless number for j-factor calculation [-]
δ	thickness [m]
γ	dimensionless number for j-factor calculation [-]
ϕ	Two-phase multiplier [-]
ρ	density [$kg \cdot m^3$]
η	efficiency [-]
μ	dynamic viscosity [$N \cdot s \cdot m^{-1}$]
ω	humidity ratio [$kg \cdot kg^{-1}$]
v	kinematic viscosity [$m^2 \cdot s^{-1}$]

Subscript

a	air
aw	air-to-wall
c	critical

cv	convective boiling
d	depth
dis	discharge
disp	displacement
exp	experiment
f	fin
H	hydraulic
Infil	infiltration
Inc	increment
L	liquid or length
Lb	lower boundary
M	mean
Mech	mechanical
N	normalized
Nb	nucleate boiling
O	out
P	primary or pitch
R	refrigerant or room
rw	refrigerant to the wall
S	secondary or supply
Sim	simulation
Std	standard deviation
Suc	suction

T	tube
Tp	two-phase
V	vapor
W	wall

Abbreviation

AEC	Annual Energy Consumption
ALR	Annual Leakage Rate
ANN	Artificial Neural Network
COMP	Compressor
COND	Condenser
COP	Coefficient of Performance
DEV	Deviation
DX	Direct Expansion
EES	Engineering Equation Solver
EOL	End of Life
EVAP	Evaporator
GWP	Global Warming Potential
HC	Hydrocarbon
HFC	Hydrofluorocarbons
HFO	Hydrofluoroolefins
HX	Heat Exchanger

LCCP	Life Cycle Climate Performance
MAC	Mobile Air Conditioning system
NREL	National Renewable Energy Laboratory
NTU	Number of Transfer Unit
PE	Power Element
RDTR	Radiator
RFD	Refrigerant Disposal Emission
RFM	Refrigerant Manufacture Emission
RPM	Revolution Per Minute
SL	Secondary Loop
TMY	Typical Meteorological Year

1 Introduction

1.1 Background

Mobile Air Conditioning system (MACs) is the air conditioning system mounted on the vehicle which helps to maintain the cabin air in the thermal comfort zone during the hot summer. Typical MACs uses R-134a as the refrigerant. However, although R-134a has no Ozone depletion potential, its Global Warming Potential (GWP) is 1430 [1], which is almost nine times of the upper boundary of the European MAC directive [2]. As a result, it has been phased out in Europe since 2017. Therefore, finding an alternative refrigerant is of great importance.

The alternative refrigerants of R-134a must have low GWP while having similar thermal properties as R-134a. The alternative refrigerants that can be found in the open literature include R-152a, R-1234yf, R-600, R-290a, and R-744. Among all those refrigerants, only R-744 is non-flammable. However, the operating pressure of R-744 is much higher than that of R-134a and therefore, requires better equipment to withstand the high pressure. While for other flammable alternatives, drop-in replacement of R-134a will put passengers in danger. Therefore, a safer system design is required. Moreover, R-1234yf is nine times expensive than R-134a [3]. So that its charge reduction is required.

The Secondary Loop (SL) system can satisfy this need. It replaces the evaporator with an intermediate heat exchanger, which isolates the refrigerant from the cabin so that the refrigerant has very little chance to get into the cabin when car crashes. In addition to providing a safe environment, the SL system can also reduce the refrigerant charge by reducing the refrigerant pipe length. Those benefits make SL system a good alternative of the conventional MACs.

1.2 Objective

The objective of this thesis is to build DX and SL air conditioning system models under both steady-state and transient conditions and simulate their performance. The steady-state model is developed in Engineering Equation Solver (EES), which is a general equation-solving program. The EES built-in thermodynamic database provides hundreds of substances as well as functions that can calculate their thermodynamic properties. The transient model is developed in Dymola, which is a transient modeling tool widely adopted by automobile and air conditioning industry. Its built-in solver can handle both partial differential equations and ordinary differential equations so that modeler can focus on dealing the underlying physics.

The steady-state and transient models of DX system are validated by the experimental data. For transient simulation, the US06 driving cycle is selected. And the performances of SL systems using R-134a, R-152a, and R-1234yf as the refrigerant are compared.

2 Literature Review

2.1 Steady-State Model of Mobile Air Conditioning System

There are two approaches to developing steady-state system model. One is the successive approach, and the other is the non-sequential approach. For successive approach, one variable is solved before the calculation moves the next variable. While for the non-sequential approach, all variables are solved together. Table 2-1 lists some steady-state system models and their model approaches.

Table 2-1: Review of Steady-State Modeling

Author	Approach	Compressor	Heat Exchanger	Ref
Davis et al. [4]	Successive	Efficiency-based	Separate zone	-
Agrawal et al. [5]	Non-sequential	Efficiency-based	-	CO_2
Richardson et al. [6]	Non-sequential	Efficiency-based	Separate zone	-
Sarkar et al. [7]	Successive	Efficiency-based	Finite volume	CO_2
Jabardo et al. [8]	Successive	Efficiency-based	Separate zone	R-134a
Lee et al. [9]	Successive	Efficiency-based	Finite volume	R-134a
Hosoz et al. [10]	Artificial neural network	-	-	R-134a

Since all variables are solved together, the non-sequential approach is more favorable for a complex system. Like the air conditioning system with internal heat exchanger. However, non-sequential approach neglects the relationship between connected cycle points, which could cause some meaningless iterations that lead to longer calculation time.

When the successive approach is implemented, modelers are always intended to write detailed mathematic equations which describe the physical meaning of the model into the system model. While for non-sequential approach, each component is treated as a black box, thus has more flexibility than the previous approach.

Davis et al. [4] proposed a steady-state system model for the refrigerant system. Mass and energy balance equations are imposed for each component. The heat exchanger is divided based on the phase of refrigerant. The condensing pressure and evaporating pressure are iterated until the condenser subcooling, and the evaporator superheat match the design targets. This model has low computational cost and therefore is suitable for design purpose.

Jabardo et al. [8] built a steady-state model for a mobile air conditioning system with variable speed compressor in EES. Each main component was modeled individually. The compressor and TXV were modeled based on curve fitted from manufacture data. For heat exchanger, it was separated into several regions which were associated with the refrigerant phase and the capacity was calculated by the ε-NTU method. The deviation of most simulation results were within 10%, and in most case, the simulation model tends to underpredict the performance of the system.

Lee et al. [9] developed an integrated model for MAC. The performance of the parallel flow condenser was predicted by empirical equations. And the evaporator model was built on the basis of overall heat transfer coefficient. Then all components were combined by mass and energy balance to create a system model. For charge comparison purpose, two system models were created. One was for adequate charge situation, and the other was for overcharge situation. For adequate charge condition, the condenser outlet was assumed to be the bubble point at the

condensing pressure. The deviation of this system model was less than 7 %. And the results indicate that 10 % overcharge is optimum for a wide range of operating condition.

In addition to the approaches mentioned above, some researchers also proposed innovative ideas to solve complex system model. Hosoz et al. [10] proposed an artificial neural network (ANN) model for MAC. ANN is a computational method which imitates human brain operating process to solve complex problems that have no algorithmic solution or are difficult to solve. To train an ANN model, experiment work is necessary. The inputs for the ANN model were compressor speed, evaporator capacity, and condenser temperature. The deviation of the system model was less than 10 % when compared to the experiment.

2.2 Transient Model of Mobile Air Conditioning System

Hendricks [11] optimized MACs using transient performance analysis. The model was built in SINDA/FLUINT, which is a software developed by National Renewable Energy Laboratory (NREL). The model had a nominal compressor model, where the compressor isentropic efficiency and volumetric efficiency were calculated from compressor pressure ratio and RPM. Both heat exchangers were serpentine type heat exchanger, and the heat transfer coefficient and pressure drop were calculated from built-in correlation. In addition to that, thermal regeneration between suction line and the expansion device was also included in the model. To link the passenger comfort with the fuel consumption, a simple cabin model which can reflect the cabin temperature and humidity change versus time were used. Single variable and dual variable optimization were done for two supplement driving cycles: US06 and SC03. The optimization result for two driving cycles differs a lot. Therefore a more sophisticated optimization strategy is needed.

Kossel et al. [12] proposed a co-simulation system model for MACs. This model was divided into sub-models, and each of them can be modeled and solved in different software. Then the system model was constructed by using co-simulation. The author created the component model by using Dymola. Although for the simple and small model, the co-simulation cost more time to simulate. When the system becomes very complex, the co-simulation model is faster and more robust compared to the close model in Dymola.

Junior [13] proposed a thermoelectric air conditioning system for automobile application. The thermoelectric air conditioning system replaced the conventional refrigerant-air heat exchanger with Peltier liquid-gas heat exchanger, where the hot side was used to heat water, and the cold side was used to cool down the air. With the help of Model Library for Thermal Components and Systems (TIL), the author was able to create the system model by connecting existing component in Dymola. The Peltier heat exchanger model was developed as a combination of a certain number of the base element. The results show that the cooling capacity provided by the HVAC system is five times higher than that of a thermoelectric device with identical power input.

Ling [14] performed steady-state and transient simulation of a R-290 secondary loop system in Dymola. This SL system replaced the evaporator with an intermediate heat exchanger and added a coolant loop on the evaporator side. The model was consists of a condenser, an intermediate heat exchanger, a compressor, a cooler and a coolant pump. The COP obtained from steady-state simulation had a 7.5% deviation. While the transient simulation demonstrated deviations less than 2.4% and 1.8% for accumulated compressor power and accumulated cooling capacity.

2.3 Alternative Refrigerants

The GWP of R-134a is 1430, which is almost nine times of the upper boundary of the GWP in the European MAC Directive [2]. Therefore, finding an alternative refrigerant is of great importance. The alternative refrigerant is expected to have similar thermal performance and has lower global warming potential. Table 2-2 lists some alternatives of R-134a. Ozone Depletion Potential is not listed here since it is 0 for all those refrigerant. The global warming potential for all those alternative refrigerants is less than 150, which is the upper boundary of the European Mac Derivative. Therefore no prohibition or additional tax will be applied to these refrigerants.

Table 2-2: Properties of Alternative Refrigerants [15]

Properties	R-134a	R-152a	R-1234yf	R-290	R-600a
Type	HFC	HFC	HFO	HC	HC
Molar Mass [kg/kmol]	102.03	66.05	114.04	44.10	58.12
Critical Temperature [°C]	101.1	113.3	94.7	96.8	135
Critical Pressure [kPa]	4,061	4,522	3,382	4,247	3,647
Normal Boiling Point [°C]	-26.11	-24.00	-29.48	-42.11	-11.78
Vapor Density (25°C) [kg/m^3]	32.35	18.47	37.93	20.62	9.13
Liquid Density (25°C) [kg/m^3]	1206.70	899.47	1091.90	492.36	550.65
Vapor Spec. Heat (25°C) [kJ/kg-K]	1.032	1.254	1.053	2.015	1.796
Liquid Spec. Heat (25°C) [kJ/kg-K]	1.425	1.800	1.392	2.719	2.430
Heat of Vaporization [kJ/kg]	177.79	279.36	145.37	335.74	328.92
Global Warming Potential (GWP)	1,430	124	4	3	3
Lower Flammability Limit [vol.%]	-	3.9	6.5	2.2	1.7
Minimum Ignition Energy [mJ]	-	0.38	>1000	0.25	0.25
Safety Group	A1	A2	A2L	A3	A3
Pricing (2017) [$ Per lb.]	7	-	66	17	15

Since R-290 and R-600a are highly flammable, this research selected R-152a and R-1234yf as alternative refrigerants.

R-152a has good thermal properties and has been widely investigated as an alternative for R-134a. Considering the fact that both R-152a and R-134 are HFC and share similar material and lubricant compatibility, Cabello et al. [16] evaluated the performance of R-152a as a drop-in replacement for R-134a in cascade refrigeration system. The cascade refrigeration system used in this research were designed for R-134a and used CO_2 on the low-temperature side. When the refrigerant was switched to R-152a, only electric expansion valve was adjusted while other components remain unchanged. Tests were performed under a wide range of operating temperature. The results show that the performance of R-134a is slightly better than that of R-152a in terms of cooling capacity. In addition to cascade refrigeration system, Cabello et al. [17] also conducted the drop-in test in a single-stage vapor compression plant equipped with a hermetic compressor. Since the liquid density of R-152a is about 25% smaller than that of R-134a, up to 41.5% reduction in refrigerant mass flow rate was observed. As a result, the reduction of cooling capacity was observed, which ranges from 1.13% to 9.75%. However, the COP of R-152a was 11.70% higher than that of R-134a.

However, R-152a is much more flammable than R-134a as it listed in Table 2-2. Therefore, it is not an appropriate candidate for drop-in replacement. One solution for this is using secondary loop system. The details about the secondary loop system is introduced in the next section. Li et al. [18] conducted experiments and simulation on the secondary loop system running R-152a. 60% charge reduction compared to R-134a was observed due to low liquid density and short pipe length. Under 35°C ambient temperature, the compressor power for R-152a system decreases by 10%, which leads to a higher COP. Under highway condition, the COP of R-152a is 5-10% higher than that of R-134a. Li also evaluated the exergy performance of both Direct Expansion (DX) and Secondary Loop (SL) system. The compressor takes the largest

portion of the exergy destruction in both systems. And for R-152a SL system, the total exergy destruction rate is 9.6% lower than that of R-134a DX system.

As a refrigerant has low GWP and has similar thermalphysical properties as R-134a, R-1234yf is considered as a potential alternative of R-134a and received lots of attention from researchers. Lee et al. [9] conducted a drop-in test for automobile heat pump system by using R-1234yf under summer and winter conditions. Water was selected as the secondary fluid for both condenser and evaporator. The results show that the discharge temperature decreases by 6.5°C and the refrigerant charge is also reduced by 10%. In addition, 4% and 2.7% of reduction were observed for capacity and coefficient of performance (COP), respectively.

Daviran et al. [19] simulated a MAC system using R-1234yf as a drop-in replacement of R-134a. The compressor was wobble plate type compressor. The condenser was mini-channel parallel-flow type heat exchanger and the evaporator was a flat-plate type heat exchanger with louver fin. LMTD method was used to analyze the performance of the heat exchanger. All refrigerant properties were obtained from REFPROP. The results showed that the heat transfer coefficient of R-1234yf was about 20% lower than that of R-134a. When the refrigerant mass flow rate was the same for R-134a and R-1234yf, the COP of the R-1234yf system was 18% higher than that of R-134a system. While when the cooling capacity was the same, the mass flow rate of the R-1234yf system was 27% higher than that of R-134a system, and the COP of the R-1234yf system was 1.3%-5% lower. In addition, the lower operating pressure was observed for R-1234yf, which indicates the potential of the thinner tube.

Navarro-Esbrí et al. [20] also conducted experiments using R-1234yf as a drop-in replacement of R-134a. Shell-and-tube heat exchangers were used as condenser and evaporator. And the secondary fluid was water and water/propylene glycol mixture for condenser and

evaporator, respectively. The cooling capacity decreased by 9%. And the volumetric efficiency of the compressor was 5% lower than that of the compressor using R-134a. The internal heat exchanger was suggested by the author to compensate the reduction of COP.

Due to smaller liquid density, the refrigerant charge for the R-1234yf system is usually smaller than that of R-134a system. Zhao et al. [21] and Wang [22] observed 5% - 10% charge reduction.

Some researchers compared several alternative refrigerants at the same time. Sánchez et al. [23] did a comparison of R-134a, R-290, R-152a, R-600a, R-1234yf, and R-1234ze in the same test facility. A hermetic-type compressor was used. Both condenser and evaporator were brazed plate heat exchanger. The secondary fluid for condenser and evaporator are water and water/propylene glycol mixture, respectively. And an electronic expansion valve was used to control the evaporator outlet superheat. Experiments were conducted under two evaporating temperatures (0 °C, -10°C) and three condensing temperature (25 °C, 35 °C, 45°C). Although 5.7% reduction of cooling capacity was observed for R-152a system, the compressor power consumption was reduced by 8.8%. Therefore, the COP actually increases by 1% - 4.8%. For the R-1324yf system, the cooling capacity was reduced by 4.5%-8.6% compared to that of R-134a system, while the compressor power consumption increased by up to 6.7%. Therefore, the COP was reduced by around 10%. For the R-290 system, up to 67% cooling capacity increment could be reached at the cost of up to 44.8% of compressor power consumption. For other refrigerants, large capacity and COP reduction were observed.

Sotomayor et al. [24] developed a semi-empirical model for MAC open piston compressor. Both pressure drop and heat transfer happened in suction and discharge were considered in the model. The characteristic parameters of the compressor model were calculated

from the R-134a test data. And then it was used to simulate R-1234yf and R-290. The results showed good agreement with the experiment, proving the model was suitable to simulate compressor with new refrigerant while the experiment data was not available.

2.4 Secondary Loop System for Mobile Air Conditioning System

SL system designed for MACs typically has only one secondary loop on evaporator side and uses R-152a [18,25–28] as refrigerant and water-glycol mixture [18,25–27,29] as secondary fluid.

Ghodbane [25,26] conducted research on the SL system using R-152a as refrigerant and ethylene glycol as secondary fluid. The chiller was a brazed aluminum plate heat exchanger. It was observed that the condenser capacity of SL system was increased by 6%, while the COP decreased by 5-19% compared to DX system. The cost of SL system was obviously higher than that of R-134a system due to additional cost for pump and pipe. But the development time of the R-152a SL system was shorter than the R-744 system.

Malvicino et al. [29] did an experimental work on an SL system using R-134a. Both condenser and evaporator were water-cooled heat exchangers. While the secondary fluid used on the evaporator side was a water-glycol mixture. The results showed that the cooling performance of the SL system during the cool down test was just slightly worse than the baseline DX system.

Eisele [27] did a thesis work on the SL system. The refrigerant used in the test was R-152a, and the secondary fluid was ethylene glycol-water mixture. Later R-290 was also evaluated by simulation. Both steady-state and transient performance were evaluated. The results showed that by using R-152a, the refrigerant charge could be reduced by 19% for DX system and 28% for SL system. And the COP of R-152a SL system was 5-10% higher than that of R-134a DX system.

3 Mobile Air Conditioning System

3.1 Direct Expansion System

The direct expansion (DX) system is the most conventional air conditioning system used in an automobile. Here, direct means that the air is directly cooled by the evaporator, while expansion refers to the isentropic expansion process the refrigerant experiences before it enters the evaporator. A DX system usually consists of four major components: compressor, condenser, expansion device and evaporator. The compressor used in this research is an electric compressor with 33 cc displacement volume. Both condenser and evaporator are microchannel heat exchanger. The condenser has one bank and four passes, while the evaporator has two banks and each bank has four passes.

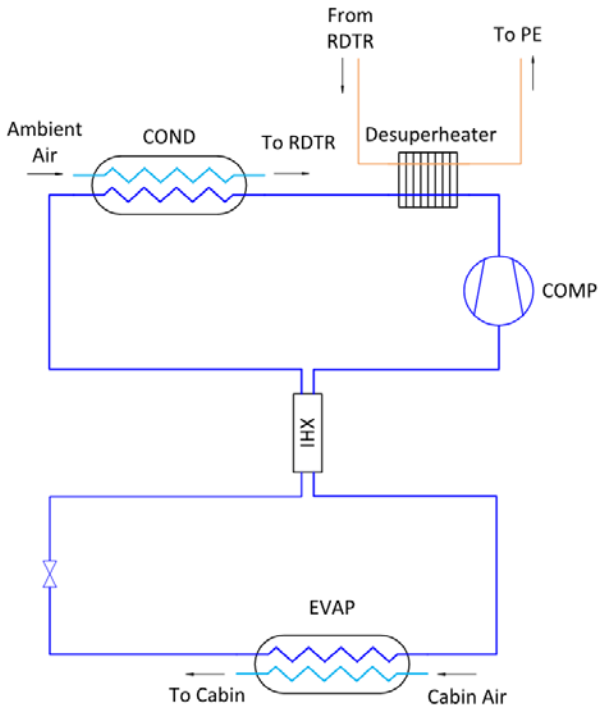

Figure 3-1: Schematic Diagram of DX System with Desuperheater

For automobile application, maintaining the power element temperature in a certain optimum operating range is also important. Therefore, in addition to the refrigerant circuit,

another coolant circuit is needed. Ethylene glycol-water mixture in 50/50 wt.% was selected as the coolant in this research due to its low freezing temperature and good thermal properties. The coolant first flow through the radiator, which is a microchannel air-refrigerant heat exchanger, to reduce its temperature. Then the relatively cold coolant is pumped to the desuperheater, which is a plate heat exchanger installed between compressor and condenser. The coolant inside desuperheater is heated by the superheated refrigerant then is lead to the power element where the coolant absorbs the dissipated heat from it.

Table 3-1: Components of DX System

Name	Type
Condenser	Microchannel HX
Evaporator	Microchannel HX
Desuperheater	Plate Heat Exchanger
Radiator	Microchannel HX

3.2 Secondary Loop System

Unlike the direct expansion system, the secondary loop system replaces the evaporator with an intermediate heat exchanger and adds one more coolant circuit on the low-pressure side. The coolant passing through the intermediate heat exchanger dissipates heat to the refrigerant and then is pumped to cabin cooler, which is an air-refrigerant heat exchanger.

The secondary loop system designed in this study replaces both condenser and evaporator with a coolant-refrigerant heat exchanger. This design not only reduces the refrigerant charge in the vehicle but also reduces the repair cost and potential of refrigerant leakage in a small accident.

Both condenser and evaporator are a compact heat exchanger with offset strip fin on the refrigerant-side and dimple fin on the coolant-side. And since the condenser now uses coolant to cool down the refrigerant, the desuperheater is also removed.

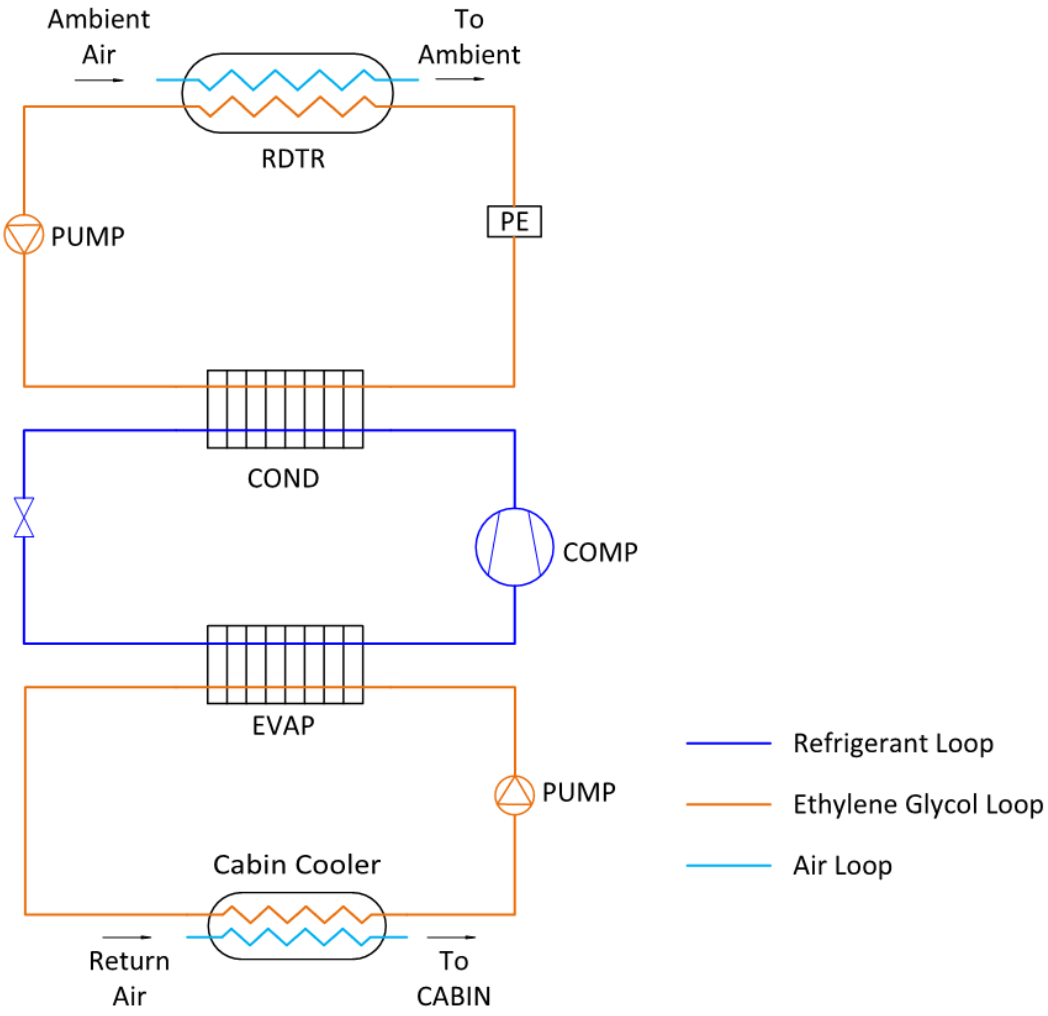

Figure 3-2: Schematic Diagram of SL System

Table 3-2: Components of SL System

Name	Type
Condenser	Compact HX(offset strip fin/dimple fin)
Evaporator	Compact HX(offset strip fin/dimple fin)
Cabin Cooler	Microchannel HX
Radiator	Microchannel HX

4 Steady-State Simulation

4.1 Modeling Approach

Steady-state models were developed for DX system and SL system in Engineering Equation Solver (EES), which is a general equation-solving program using declarative modeling language. Unlike imperative language, it does not require the developer to specifically define the calculation flow. Instead, the behavioral relationships between each parameter need to be defined for the solver to find solution algorithm. At the same time, variable constraints are necessary in some cases to eliminate unphysical solutions.

Since "if-statement" is necessary for heat exchanger calculation which unfortunately is not supported in the EES main program, each component was built in the internal procedure in the very beginning of the program. Then those procedures are called in the main program to assemble a complete system model.

4.1.1 Components

4.1.1.1 Compressor

The compressor model is a semi-empirical model. The compressor mass flow rate is calculated by the suction density, the compressor displacement volume, the revolution per minute (RPM) and volumetric efficiency. The equation is as follows:

$$\dot{m} = \frac{V_{disp} \times RPM \times \rho_s \times \eta_v}{60} \tag{4-1}$$

The volumetric efficiency and isentropic efficiency are calculated by the normalized polynomial equations fitted from the experimental data provided by the manufacturer. These polynomials are a function of normalized RPM and pressure ratio (PR) as follows:

$$\eta_{vol} = 0.9556 + 0.01914 \times RPM_n - 0.04078 \times PR_n - 0.02483 \times RPM_n^2 + 0.01205 \times RPM_n \times PR_n - 0.009553 \times PR_n^2 \quad (4\text{-}2)$$

$$\eta_{isen} = 0.7045 - 0.02539 \times RPM_n + 0.01043 \times PR_n - 0.00987 \times RPM_n^2 + 0.02331 \times RPM_n \times PR_n - 0.02449 \times PR_n^2 \quad (4\text{-}3)$$

where n refers to normalized value, which is calculated as follows:

$$RPM_n = \frac{RPM - RPM_m}{RPM_{std}} \quad (4\text{-}4)$$

$$PR_n = \frac{PR - PR_m}{PR_{std}} \quad (4\text{-}5)$$

Then the compressor work can be calculated by the following equation:

$$W = \frac{\dot{m} \times (h_{dis} - h_{suc})}{\eta_{mech}} \quad (4\text{-}6)$$

where h stands for the enthalpy of the refrigerant and η_{mech} is the mechanical efficiency of the compressor which is calculated by the following equation:

$$\eta_{mech} = 0.7048 + 0.004631 \times PR + 6.255e^{-5} \times RPM - 0.003303 \times PR^2 + 3.216e^{-6} \times PR \times RPM - 6.369e^{-9} \times RPM^2 \quad (4\text{-}7)$$

4.1.1.2 Condenser

The condenser is a microchannel heat exchanger. The heat exchanger model was first built in CoilDesigner, a heat exchanger simulation software developed by the Center for Environment Energy Engineering, University of Maryland. The deviation of the condenser capacity calculated by the CoilDesigner model is less than 2%. Then a parametric study was performed to create the heat exchanger performance map. Condenser inlet pressure, condenser inlet superheat and refrigerant mass flow rate are three changing variables. Each variable has ten runs and 1,000 runs in total, as shown in Table 4-1. The results of the parametric study were exported into a CSV file which can be read by EES. Once the data is loaded by EES, the

program will transform the output into a three dimension array. Then the performance of condenser can be calculated by doing linear interpolation between nearby points.

Table 4-1: Condenser Parametric Study Variables

Variables	Lower Boundary	Upper Boundary	Runs
$T_{cond,in,sup}$ [°C]	0	20	10
$P_{cond,in}$ [kPa]	800	2400	10
$\dot{m}_r$ [kg/s]	0.02	0.06	10

Take condenser capacity calculation as an example. The capacity map is loaded as a three dimension array, like Q$[x_1, x_2, x_3]$. Where $x_1, x_2,$ and x_3 is the index of condenser inlet superheat, refrigerant mass flow rate and condenser inlet pressure, respectively. They are calculated in the beginning of the procedure and are integers ranging from 1 to 10. Once the heat exchanger model is called by the main program, the heat exchanger model will first calculate the $x_1, x_2,$ and x_3 by the following equation:

$$x_i = trunc(\frac{y_{in} - y_{lb}}{y_{int}}) \tag{4-8}$$

where lb stands for lower boundary and int stands for interval. The y here refers to the variables represented by the index. For example, y is condenser inlet superheat for x_1. And the trunc() function will round the number inside the brackets toward zero therefore the output must be an integer.

Once the index is calculated, the program can start doing interpolation by using the following set of equations:

$$\dot{Q}_1 = \dot{Q}[x_1, x_2, x_3] + \frac{\dot{m}_{inc}}{\dot{m}_{int}}(\dot{Q}[x_1 + 1, x_2, x_3] - \dot{Q}[x_1, x_2, x_3]) \tag{4-9}$$

$$\dot{Q}_2 = \dot{Q}[x_1, x_2, x_3 + 1] + \frac{\dot{m}_{inc}}{\dot{m}_{int}}(\dot{Q}[x_1 + 1, x_2, x_3 + 1] - \dot{Q}[x_1, x_2, x_3 + 1]) \quad (4\text{-}10)$$

$$\dot{Q}_3 = \dot{Q}_1 + \frac{P_{inc}}{P_{int}}(\dot{Q}_2 - \dot{Q}_1) \quad (4\text{-}11)$$

$$\dot{Q}_4 = \dot{Q}[x_1, x_2 + 1, x_3] + \frac{\dot{m}_{inc}}{\dot{m}_{int}}(\dot{Q}[x_1 + 1, x_2 + 1, x_3] - \dot{Q}[x_1, x_2 + 1, x_3]) \quad (4\text{-}12)$$

$$\dot{Q}_5 = \dot{Q}[x_1, x_2 + 1, x_3 + 1] + \frac{\dot{m}_{inc}}{\dot{m}_{int}}(\dot{Q}[x_1 + 1, x_2 + 1, x_3 + 1] - \dot{Q}[x_1, x_2 + 1, x_3 + 1]) \quad (4\text{-}13)$$

$$\dot{Q}_6 = \dot{Q}_4 + \frac{P_{inc}}{P_{int}}(\dot{Q}_5 - \dot{Q}_4) \quad (4\text{-}14)$$

$$\dot{Q} = \dot{Q}_3 + \frac{T_{inc}}{T_{int}}(\dot{Q}_6 - \dot{Q}_3) \quad (4\text{-}15)$$

Since now the condenser refrigerant-side capacity and pressure drop are known, the condenser outlet enthalpy can be calculated by simple calculation. The drawback of this model is that each time when the air-side inlet condition changes the parametric table must be created again.

4.1.1.3 Evaporator

Table 4-2: Evaporator Parametric Study Variables

Variables	Lower Boundary	Upper Boundary	Runs
$x_{evap,in}$ [-]	0.1	0.4	10
$P_{evap,in}$ [kPa]	200	500	10
$\dot{m}_r$ [kg/s]	0.02	0.05	10

The evaporator is also a microchannel heat exchanger. Same as condenser model, the evaporator model is first built in CoilDesigner. The deviation of the evaporator capacity calculated by the CoilDesigner model is less than 8%. As shown in Table 4-2, the changing

variables used in the parametric study for evaporator are evaporator inlet quality, refrigerant mass flow rate and evaporator inlet pressure. Unlike condenser model, the evaporator model sometimes requires back calculation in the system model. An interpolation model like condenser model is not efficient enough in that case. Therefore, part of the interpolation is replaced with polynomial fitted from the parametric study data. Since it is difficult to create a polynomial with three variables, ten polynomials with evaporator inlet quality and pressure as variables were created. Each polynomial can predict the system performance under certain mass flow rate. Then the current performance can be calculated by using the following interpolation:

$$\dot{Q} = \dot{Q}[x] + \frac{\dot{m}_{inc}}{\dot{m}_{int}}(\dot{Q}[2] - \dot{Q}[1]) \tag{4-16}$$

Other parameters like pressure drop can also be interpolated by this equation. The only thing needs to be done is replacing $\dot{Q}$ with the name of the new parameter, i.e. dp.

For air side calculation, it is separated from the refrigerant side calculation and is written in an individual procedure which also uses interpolation like condenser model.

4.1.1.4 Internal Heat Exchanger

In the DX system, an internal heat exchanger is installed to enhance condenser outlet subcooling and evaporator outlet superheat. The model was developed by using finite volume method. The internal heat exchanger is evenly divided into three segments. Inside each segment, the capacity is calculated by the ε-NTU method. Since inside the internal heat exchanger, the high-pressure side only has subcooled liquid, and the low-pressure side only has superheated vapor, only single phase transfer is involved in the internal heat exchanger, which makes the model simpler.

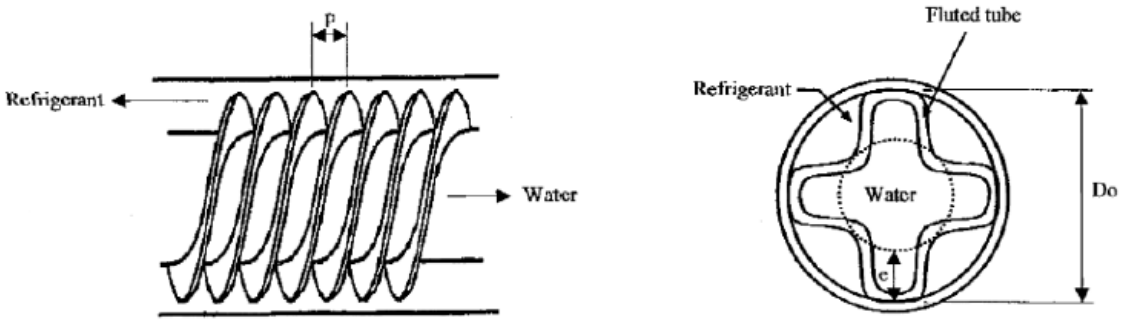

Figure 4-1: Internal Heat Exchanger Geometry[30]

For the internal heat exchanger in this study, the outer tube is smooth tube and the inner tube is a fluted tube. Figure 4-1 shows the definition of the internal heat exchanger geometry. The actual surface area and volume of the inner tube are very difficult to calculate due to lack of information. Therefore, the geometry of the inner tube is simplified to be a combination of several periodic segments, which consists of two conical frustums. After simplification, the surface area of one fluted tube segment can be calculated by the following equation:

$$A = 2\pi(D_i - e)\sqrt{e^2 + (\frac{p}{2})^2} \tag{4-17}$$

And the volume of each periodic segment can be calculated by:

$$V_{in} = \frac{\pi p}{3}(\left(\frac{D_i}{2}\right)^2 + \left(\frac{D_i}{2} - e\right)^2 + \frac{D_i}{2}(\frac{D_i}{2} - e)) \tag{4-18}$$

Then the volumetric diameter of the inner tube can be obtained by the following equation:

$$D_{vi} = \sqrt{\frac{4V_{in}}{\pi L}} \tag{4-19}$$

To obtain the hydraulic diameter of the outer tube, the outer volumetric diameter is also needed, which is defined as:

$$D_{vo} = D_{vi} + 2\delta \tag{4-20}$$

Then, the hydraulic diameter of the circular tube can be calculated by the following equation:

$$D_h = D_{o,i} + D_{vo} \tag{4-21}$$

The outer volumetric diameter is also used to calculate the helix angle, which is defined as:

$$\theta = \arctan(\frac{\pi D_{vo}}{Np}) \tag{4-22}$$

where N is the number of flute starts at any cross-section.

To describe the thermal performance of the internal heat exchanger, some dimensionless numbers are required. They are defined as follows:

$$e^* = \frac{e}{D_{vi}} \tag{4-23}$$

$$p^* = \frac{p}{D_{vi}} \tag{4-24}$$

$$\theta^* = \frac{\theta}{D_{vi}} \tag{4-25}$$

Then the single phase heat transfer coefficient can be calculated by the correlation proposed by Arnold et al. [31].

$Re \leq 5{,}000$

$$Nu = 0.014Re^{0.842}(e^*)^{-0.067}(p^*)^{-0.293}(\theta^*)^{-0.705}Pr^{0.4} \tag{4-26}$$

$Re > 5{,}000$

$$Nu = 0.064Re^{0.773}(e^*)^{-0.242}(p^*)^{-0.108}(\theta^*)^{0.599}Pr^{0.4} \tag{4-27}$$

Then the UA can be calculated as follows:

$$\frac{1}{UA} = \frac{1}{h_i A_i} + \frac{\log(\frac{D_o + 2\delta}{D_i})}{2\pi kL} + \frac{1}{h_o A_o} \tag{4-28}$$

The number of the transfer unit (NTU) is defined as:

$$NTU = \frac{UA}{C_{min}} \tag{4-29}$$

where C_{min} is minimum heat capacity rate, which is the product of specific heat capacity and mass flow rate.

Therefore the ε is calculated by the following counter flow equation:

$$\varepsilon = \frac{1 - \exp[-NTU(1 - C_r)]}{1 - C_r \exp[-NTU(1 - C_r)]} \tag{4-30}$$

where C_r is the ratio of maximum heat capacity rate over minimum heat capacity rate.

Thus the capacity can be calculated by multiply ε with the maximum capacity that is available. To simplify the calculation, the pressure drop of the refrigerant is modeled as a function of mass flow rate.

$$dp = dp_0 (\frac{\dot{m}}{\dot{m}_0})^2 \tag{4-31}$$

where dp_0 and $\dot{m}_0$ come from experiment data.

As shown in Figure 4-2. The calculation of internal heat exchanger model starts from guessing the outlet temperature and pressure of the outer tube. So the capacity of the inner and outer tube, as well as the outlet condition of the inner tube and inlet condition of the outer tube, can be calculated. The inner tube outlet condition of the previous segment becomes the inner tube inlet condition of the next segment, and the inlet condition of the outer tube becomes the outer tube outlet condition of the next segment. The calculation will continue until the segment index reaches its maximum value. Then the model will check the residual of the inlet

temperature and pressure of the outer tube. If the residual is larger than the threshold, iteration will be performed.

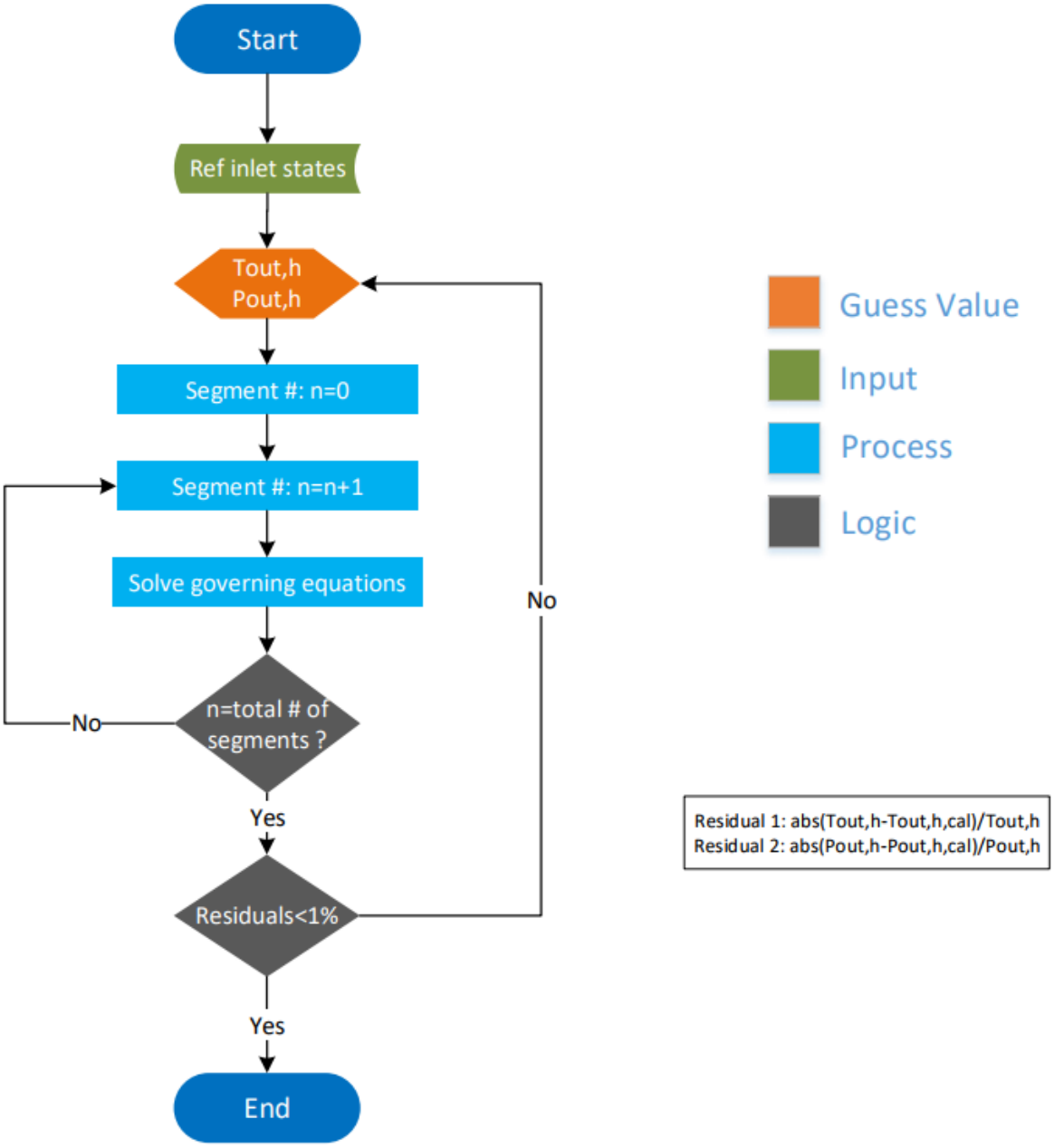

Figure 4-2: Calculation Flowchart of Internal Heat Exchanger Model

4.1.1.5 Compact Heat Exchanger

The compact heat exchanger is used in the SL system as condenser and evaporator. Based on the flat plate heat exchanger, offset strip fin (Figure 4-3) is added on the refrigerant-side and dimple fin is added on the coolant side.

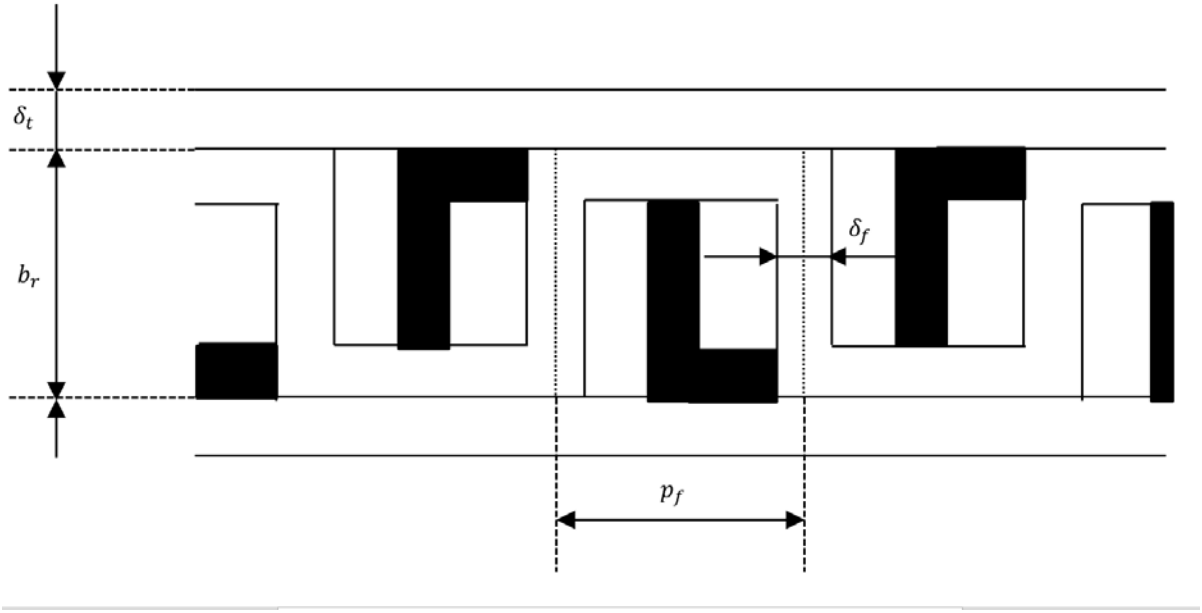

Figure 4-3: Offset Strip Fin Geometry

For the refrigerant side, the primary heat exchanger area can be calculated by the following equation:

$$A_p = 2W_t L_t - 2\delta_f L_t n_f + 2bL_t \tag{4-32}$$

where W_t is the tube width, L_t is the tube length and n_f is the number of fins. The first term is the tube internal surface area, the second term is the fin base area and the third term is the passage wall area.

Then the fin area can be calculated as follows:

$$\begin{aligned} A_s = {} & 2(b-\delta_f)L_t n_f + 2(b-\delta_f)\delta_f n_{off} n_f \\ & +(p_f-\delta_f)\delta_f(n_{off}-1)n_f + 2p_f\delta_f n_f \end{aligned} \tag{4-33}$$

where n_{off} is the number of offset fin. The first term is the fin surface area, the second term is the offset strip fin edge area, the third term is the internal offset strip fin edge area and the last term is the sum of the first and the last offset strip fin edge area.

And the cross-sectional area is obtained by:

$$A_c = (b - \delta_f)(p_f - \delta_f)n_f \tag{4-34}$$

The hydraulic diameter of the refrigerant channel can be calculated by the following equation:

$$D_h = \frac{4A_c L_t}{A_p + A_s} \tag{4-35}$$

Unlike internal heat exchanger, both single-phase and two-phase refrigerant exist in the compact heat exchanger. Therefore, two types of segment calculation, one for single phase and one for two-phase, are needed. The inputs and outputs for both segments are the same, and the difference only lies on the calculation of heat transfer coefficient, pressure drop and ε.

For single-phase segment, the heat transfer coefficient is calculated by using Chilton and Colburn j-factor. The correlation used in this model was proposed by Manglik et al. [32], which is as follows:

$$\begin{aligned} j = {} & 0.6522Re^{-0.5403}\alpha^{-0.1541}\beta^{0.1499}\gamma^{-0.0678} \\ & \times [1 + 5.269 \times 10^{-5}Re^{1.34}\alpha^{0.504}\beta^{0.456}\gamma^{-1.055}]^{0.1} \end{aligned} \tag{4-36}$$

where α, β and γ are dimensionless number and are defined as follows:

$$\alpha = \frac{p_f - \delta_f}{b - \delta_f} \tag{4-37}$$

$$\beta = \frac{\delta_f}{l_f} \tag{4-38}$$

$$\gamma = \frac{\delta_f}{p_f - \delta_f} \tag{4-39}$$

where p_f is fin pitch and l_f is fin length.

Then the heat transfer coefficient can be calculated by the definition of j-factor.

$$h = \frac{jRePr^{1/3}k}{D_h} \tag{4-40}$$

Then the heat transfer coefficient will be used to calculate the fin efficiency by using the following equation:

$$L_f = \frac{b}{2} - \delta_f \tag{4-41}$$

$$m = \sqrt{\frac{2h}{k_f \delta_f}(1 + \frac{\delta_f}{l_f})} \tag{4-42}$$

$$\eta_f = \frac{tanh(mL_f)}{mL_f} \tag{4-43}$$

The overall heat transfer area is the sum of the primary heat transfer area and effective fin area:

$$A = A_p + \eta_f A_s \tag{4-44}$$

The fanning friction factor proposed by Manglik et al. [32] is used to calculate the pressure drop of the refrigerant:

$$f = 9.6243Re^{-0.7422}\alpha^{-0.1856}\beta^{0.3053}\gamma^{-0.2659} \times [1 + 7.669 \times 10^{-8}Re^{4.429}\alpha^{0.920}\beta^{3.767}\gamma^{0.236}]^{0.1} \tag{4-45}$$

Then the pressure drop of refrigerant can be calculated by the following equation:

$$\Delta P_{sp} = f\frac{L}{R}\rho u^2 \tag{4-46}$$

For the two-phase segment, when the refrigerant is boiling, the heat transfer coefficient is consists of two parts, one is nucleate boiling heat transfer coefficient, and one is convective

boiling heat transfer coefficient. The nucleate boiling heat transfer coefficient is calculated by the correlation proposed by Nishikawa et al. [33]:

$$h_{nb} = Sh_{pb} \tag{4-47}$$

$$h_{pb} = 31.4[\frac{p_c^{0.2}F_p}{M^{0.1}T_c^{0.9}}]q''^{0.8} \tag{4-48}$$

$$F_p = \frac{(p/p_c)^{0.23}}{[1.0 - 0.99(p/p_c)]^{0.9}} \tag{4-49}$$

where the suppression factor S is proposed by Bennett et al. [34]:

$$S = \frac{24.4}{N_B}[1 - \exp(-0.041N_B)] \tag{4-50}$$

$$N_B = \frac{h_f}{k_f}[\frac{\sigma}{g(\rho_f - \rho_g)}]^{0.5} \tag{4-51}$$

where p_c is critical pressure, T_c is critical temperature, M is the molecular weight , q'' is heat flux and σ is surface tension.

For the convective boiling heat transfer coefficient, it is the product of Reynold number factor F and liquid heat transfer coefficient. The F is calculated by the correlation developed by Kim et al. [35]:

$$h_{cb} = Fh_f \tag{4-52}$$

$$F = [1 + \frac{2.52}{X^{0.5}} + \frac{15.1}{X^2}] \tag{4-53}$$

Therefore, the heat transfer coefficient can be calculated by adding convective boiling heat transfer coefficient and nucleate boiling heat transfer coefficient.

Since there is no correlation available for condensation heat transfer coefficient using offset strip fin, I first calculated the boiling heat transfer coefficient and condensation heat transfer coefficient for one plate heat exchanger. Then divided the boiling heat transfer by the

condensation heat transfer, thus get a ratio. And then I curve fitted the ratio as a function of saturating pressure and refrigerant quality. Then the condensation heat transfer coefficient for offset strip fin was obtained by dividing boiling heat transfer by the ratio.

As mentioned above, the ratio is calculated by dividing boiling heat transfer coefficient for plate heat exchanger by condensation heat transfer coefficient for plate heat exchanger. The boiling heat transfer coefficient for plate heat exchanger is calculated by the correlation developed by Amalfi et al. [36], which is as follows:

$Bd < 4$

$$h = 982(\frac{k_l}{D_h})\left(\frac{\beta_p}{\beta_{p,max}}\right)^{1.101}\left(\frac{G^2 D_h}{\rho_m \sigma}\right)^{0.315}(\frac{\rho_l}{\rho_g})^{-0.224} Bo^{0.320} \tag{4-54}$$

$Bd \geq 4$

$$h = 18.495(\frac{k_l}{D_h})\left(\frac{\beta_p}{\beta_{p,max}}\right)^{0.248}\left(\frac{xGD_h}{\mu_g \sigma}\right)^{0.135}\left(\frac{GD_h}{\mu_l}\right)^{0.351}\left(\frac{\rho_l}{\rho_g}\right)^{0.223} Bo^{0.320} \tag{4-55}$$

where

$$Bd = \frac{(\rho_l - \rho_g) g D_h^2}{\sigma} \tag{4-56}$$

$$Bo = \frac{q''}{F\gamma_p} \tag{4-57}$$

The condensation heat transfer coefficient for plate heat exchanger is calculated by the correlation proposed by Yan et al. [37] as follows:

$$h = 4.118(\frac{k_l}{D_h}) Re_{eq}^{0.4} Pr_l^{1/3} \tag{4-58}$$

where,

$$Re_{eq} = \frac{D_h}{\mu_l} G[(1-x) + x(\frac{\rho_l}{\rho_g})^{0.5}] \tag{4-59}$$

The ratio was normalized and fitted as a polynomial as shown in Figure 4-4.

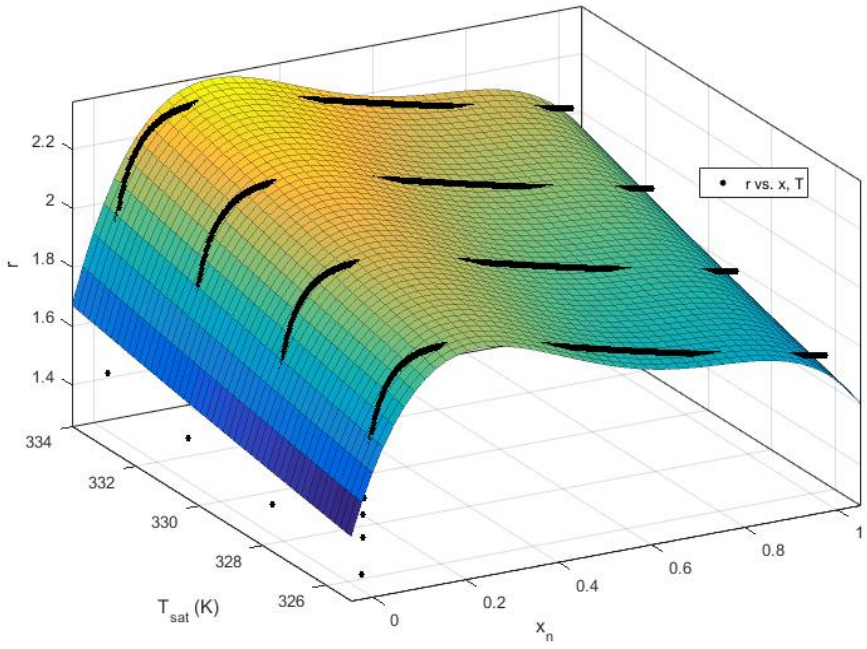

Figure 4-4: Ratio of $h_{boiling}$ over h_{cond}

The pressure drop of the two-phase segment is calculated by multiply the liquid pressure drop with two-phase multiplied proposed by Kim et al. [35], which is defined as:

$$\phi_r^2 = 1 + \frac{23.4}{X} + \frac{4.17}{X^{2.66}} \tag{4-60}$$

where X is Martinelli number [38] and is defined as:

$$X = \frac{(1-x)}{x}\left[\frac{f_l}{f_v}\frac{v_l}{v_v}\right]^{1/2} \tag{4-61}$$

Therefore the refrigerant two-phase pressure drop is obtained by:

$$\Delta p_{tp} = \phi_r^2 \Delta p_l \tag{4-62}$$

For the coolant side, dimple fin (Figure 4-5) is added on the flat plate. The dimple is modeled as a circular truncated cone.

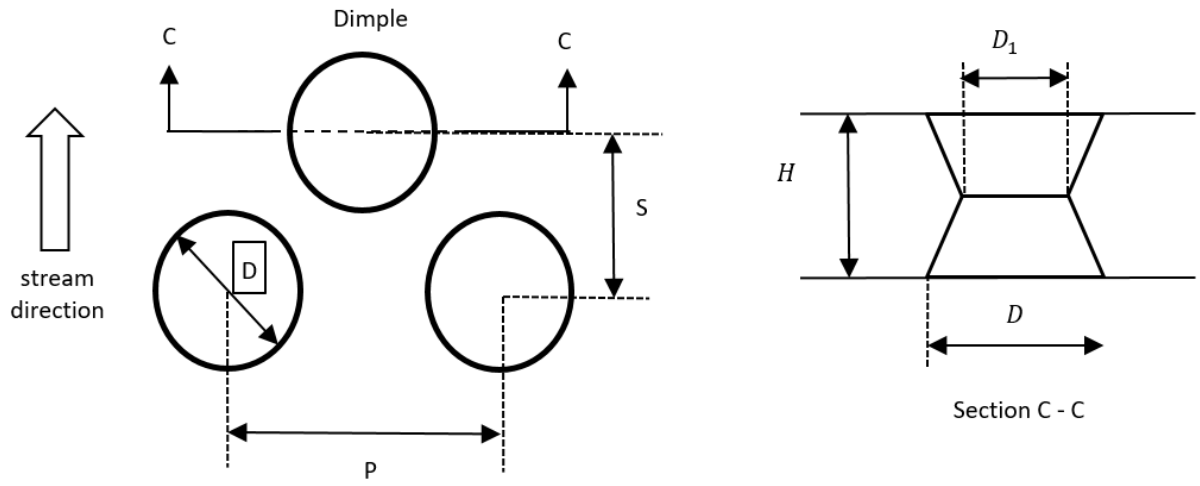

Figure 4-5: Dimple Fin Geometry

The cross section area of the coolant channel is calculated by the following equation:

$$A_c = \frac{(W \times H + W \times H - (D + D_1)\frac{H}{2} floor(\frac{W}{S}))}{2} \tag{4-63}$$

where "floor" function returns the integer part of the argument and discards the part. The number of the dimple can be calculated by using the following equation:

$$nod = floor\left(\frac{W}{P}\right) \times floor\left(\frac{L}{S}\right) - floor\left(\frac{L}{S}\right)/2 \tag{4-64}$$

The volume of each set of dimple is defined as

$$V_{dimp} = 2\frac{\pi}{3}\frac{H}{2}\frac{(D^2 + D_1^2 + DD_1)}{4} \tag{4-65}$$

Therefore, the channel volume can be calculated from the following equation

$$V = W \times L \times H - V_{dimp} nod \tag{4-66}$$

And the equation for hydraulic diameter is as follows

$$D_h = \frac{4V}{A_s} \tag{4-67}$$

The calculation of the heat transfer coefficient of the coolant depends on its Reynold number. The coolant selected in this research is ethylene-glycol water mixture with 50/50 wt.% concentration. Due to the high viscosity of the ethylene glycol, in most case, the coolant flow inside the channel is laminar flow. Therefore, the fixed Nusselt number 7.541 for fully developed laminar flow in the parallel plate was selected. In the case of larger Reynold number occurs, the correlation proposed by Metzger et al. [39] is also used:

$\mathrm{Re}<1{,}100$

$$Nu = 7.541 \tag{4-68}$$

$1{,}100<\mathrm{Re}<110{,}000$

$$Nu = 0.21Re^{0.69} \tag{4-69}$$

Then for single-phase segment, the ε can be calculated by the equation (4-30). And for the two-phase segment, the ε is calculated by the equation below

$$\varepsilon = 1 - \exp(-NTU) \tag{4-70}$$

Since pressure is not an input for most property functions of ethylene glycol mixture and the pressure drop calculation has high computational cost, the coolant pressure is fixed at atmospheric pressure and the pressure drop on the coolant side was ignored.

Similar to the internal heat exchanger model, the calculation starts from guessing the outlet condition of one side as shown in Figure 4-6. The coolant side outlet is selected as the guessing point because of its simplicity. Since the pressure drop of coolant side is ignored, only outlet temperature needs to be guessed. Then the model will determine whether to solve single-phase segment or two-phase segment based on the refrigerant inlet condition. Once the segment is solved, the outlet quality will be compared with the inlet quality as well as 0 and 1. If the inlet quality is larger than 1 and the outlet quality is less than 1 or vice versa, then phase change

occurs inside the segment. In this case, the previous calculation is no longer accurate. To increase the accuracy of the model, segments are inserted into that specific segment.

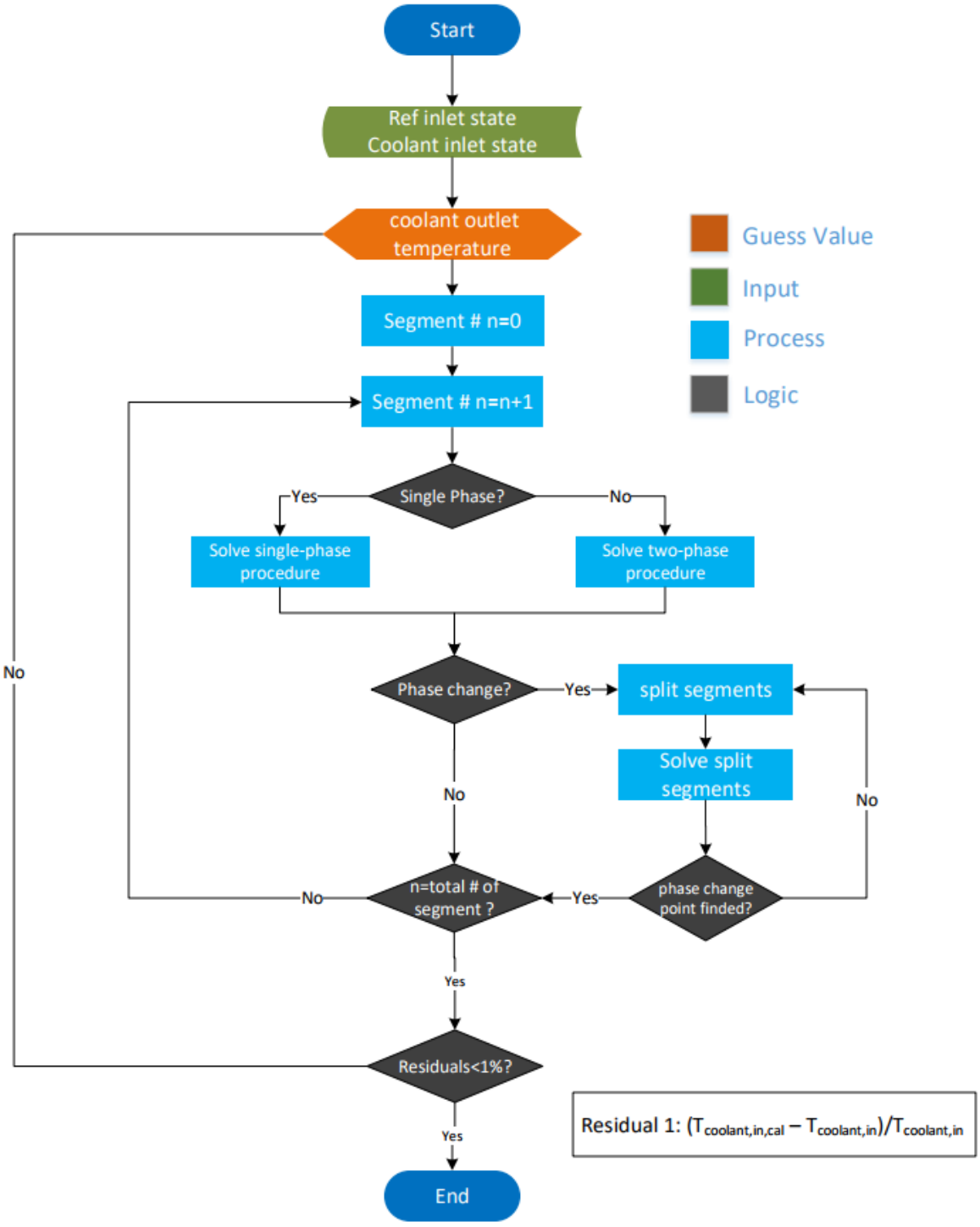

Figure 4-6: Calculation Flowchart for Compact Heat Exchanger

This process continues until the outlet quality of one of the inserted segment is close to the phase change point, where the quality is 1 for single-phase to two-phase and 0 for two-phase to single-phase. Once the phase change point is located, this segment will be divided into two parts associated with their states of refrigerant. Their capacities will be calculated separately. And the capacity of the whole segment can be obtained by summing them together. Then the model continues to solve the next segment until the segment number index reaches the maximum value. Then the coolant inlet temperature calculated by the model, which is the inlet temperature for the last segment, is compared to the actual coolant inlet temperature. Iteration is performed if the residual larger than the threshold which is 1%.

4.1.1.6 Desuperheater

The desuperheater is very similar to the compact heat exchanger. They both use offset strip fin on the refrigerant side. But unlike the compact heat exchanger, the coolant side for the desuperheater only has a small number of dimple, therefore, is considered as a flat plate. Besides, differ from the counter flow arrangement used in the compact heat exchanger, the flow arrangement of the desuperheater is cross flow.

The refrigerant-side calculation is the same as the compact heat exchanger model, therefore, is skipped in this section for brevity.

The coolant side calculation is much simpler. Since it is modeled as a flat plate, the cross section area of the coolant channel is the product of the channel width and channel height. And the hydraulic diameter is calculated by its definition.

Since it is cross flow, the ε is calculated by the following equation

$$\epsilon = \left(\frac{1}{C_r}\right)(1 - \exp\{-C_r[1 - \exp(-NTU)]\}) \tag{4-71}$$

The model calculation flow is similar to the internal heat exchanger and therefore is skipped in this section.

4.1.2 Systems

4.1.2.1 Steady-State Model for DX System

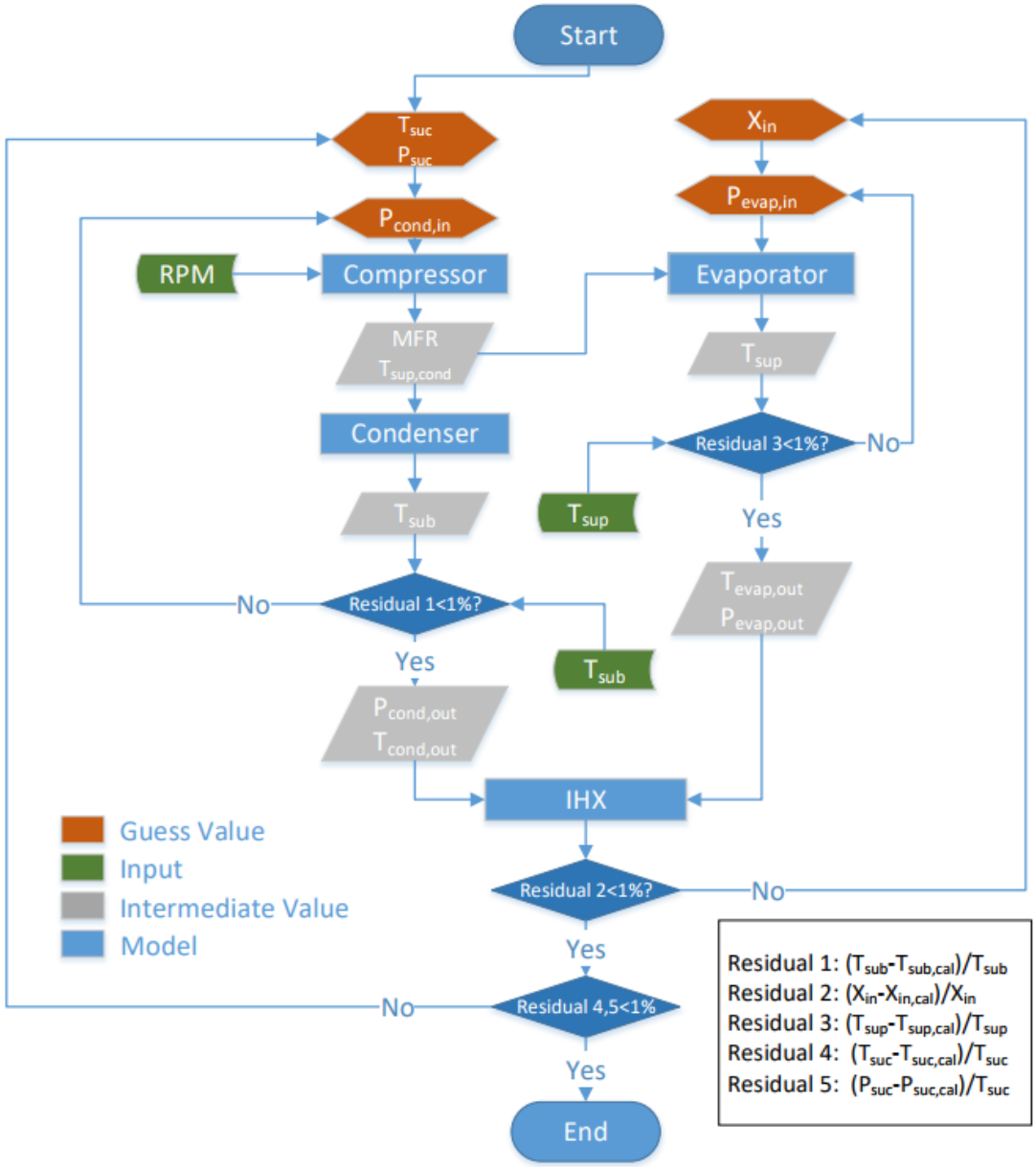

Figure 4-7: Calculation Flowchart for DX System Model

As shown in Figure 4-7, the calculation starts from compressor suction point. The model first guesses the suction temperature, pressure as well as discharge pressure. And since the compressor RPM is already known, the refrigerant mass flow and compressor discharge temperature can be calculated by the compressor model. Once that is done, two calculations start simultaneously. One is high-pressure side and the other is low-pressure side. For the high-pressure side calculation, since the desuperheater refrigerant inlet state and refrigerant mass flow rate is known, the desuperheater model can calculate its performance and refrigerant outlet state, which is also the inlet state for the condenser. Through condenser model, the condenser refrigerant outlet state can be calculated. And this becomes the input of the internal heat exchanger model outer tube. And for the low-pressure side calculation, the model first guesses the evaporator inlet quality and pressure, then the evaporator outlet state can be calculated by the evaporator model. The calculated superheat is compared with the superheat set by the user. If their difference is larger than 1%, the evaporator pressure will be updated. Iteration will continue until it satisfies the convergence requirement. With that information, the internal heat exchanger can calculate the evaporator inlet quality and compressor suction state. Since now all the state points are known, the model will compare two sets of data: the evaporator inlet quality calculated by internal heat exchanger model and the quality calculated by evaporator model, the condenser outlet subcooling calculated by condenser model and the given target subcooling. The model will keep iteration until the deviation is smaller than the threshold.

4.1.2.2 Steady-State Model for SL System

The inputs for the secondary loop system are the coolant inlet state for both condenser and evaporator, the condenser outlet subcooling, evaporator outlet superheats and compressor RPM.

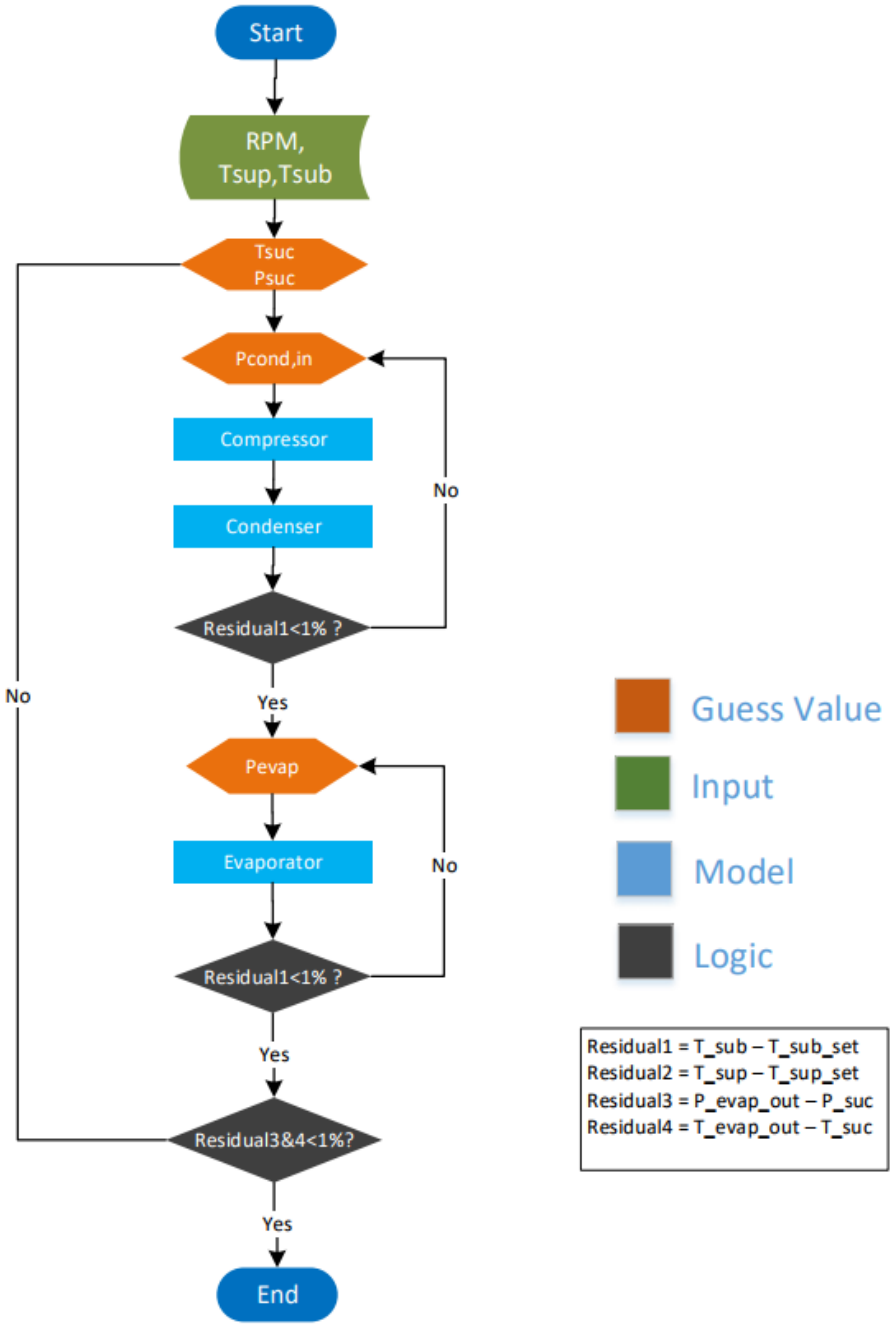

Figure 4-8: Calculation Flowchart for SL System Model

As shown in Figure 4-8. The calculation starts from guessing the suction temperature and pressure, as well as the discharge pressure. Then the compressor model will calculate the refrigerant mass flow rate based on the suction density calculated from the suction state and

compressor RPM. The refrigerant inlet temperature and pressure, plus the coolant inlet state are passed into the condenser model, which then returns its capacity and refrigerant outlet state.

The calculated subcooling of condenser is then compared to the subcooling set by the user. If their difference is larger than 1 %, the compressor discharge pressure will be adjusted by using the Broyden's method, which is a quasi-Newton method using the finite difference to approximate the derivative. This process will continue until the difference between calculated subcooling and input subcooling is less than 1%.

Then the system model will guess the evaporating pressure. Since the evaporator refrigerant inlet enthalpy is the same as the condenser outlet enthalpy, the evaporator refrigerant inlet quality can be calculated. Then these information becomes the input for the evaporator model. The evaporator model will calculate its capacity and refrigerant outlet state. The calculated superheat will then be compared to the given superheat.

The output of the evaporator model will be compared to the suction state. If the difference is larger than the threshold, iteration will be performed. Similar to condensing side, if their difference is larger than 1%, then the evaporator inlet pressure will be adjusted by using the Broyden's method. Iteration will continue until the deviation is less than 1%.

Finally, the evaporator outlet state is compared to the compressor suction state. If their difference is less than 1%, simulation is considered to be finished and the results will be returned. Otherwise, the suction temperature and pressure will be updated with the value calculated from the evaporator model.

4.2 Simulation Results

4.2.1 DX System

Three tests were conducted of the DX system. The test condition is listed in Table 4-3. Test 1 represents typical driving condition during summer where the ambient temperature is 35°C and the vehicle speed is 50 kilometers per hour (kph). While Test 2 represents the driving condition in the highway where the vehicle speed reaches 100 kph. For Test 3, its ambient temperature is 10 K higher than other two cases. The air inside cabin has lower relative humidity than others, which means lower latent load. The vehicle speed in Test 3 is 50 kph which is the same as Test 1.

Table 4-3: Test Conditions for DX system

Parameters	Test 1	Test 2	Test 3
$T_{cond,air,in}$ [°C]	35	35	45
$VFR_{cond,air,in}$ [SCMH]	2,246	3,607	2,246
$T_{evap,air,in}$ [°C]	35	35	35
$VFR_{evap,air,in}$ [SCMH]	451	451	451
$RH_{evap,air,in}$ [%]	40	40	25
$T_{cond,sub}$ [K]	20	18	23
$T_{evap,sup}$ [K]	8	8	7
Compressor RPM	5,000	5,000	8,000

The simulation results are shown in Figure 4-9 through Figure 4-13. As shown in Figure 4-10, the EES system model shows good accuracy in terms of cooling capacity. The largest deviation is 1.2%. It is observed from the Figure 4-13 that the internal heat exchanger model has the largest deviation among other components. This is mainly caused by two reasons. First, the internal heat exchanger model uses simplified geometry model to calculate the heat transfer area, which may lead to large deviation compared to details model like other heat exchangers. The second reason is that the experimental capacity of the internal heat exchanger was calculated

from the compressor suction port and the evaporator inlet, which means the heat loss through the pipe was also included in the model. However, the heat loss through the pipe was not considered in the model, which also leads to the large deviation.

As shown in Figure 4-9, Figure 4-11 and Figure 4-12, large deviation was observed for the Test 3. This is because the compressor RPM of Test 3 is 8,000, which is much higher than the other two tests. And since the compressor efficiency curve was fitted with the data ranging from 3,000 to 7,000, it is reasonable to believe that the efficiency of compressor model would have higher deviation than the other tests. Although the condenser capacity of Test 3 is over predicted by around 5%, its side effect is offset by the under predicted capacity of desuperheater model. Therefore the deviation of the evaporator inlet quality is only 0.1%. As a result, the evaporator model shows good accuracy compared to other components.

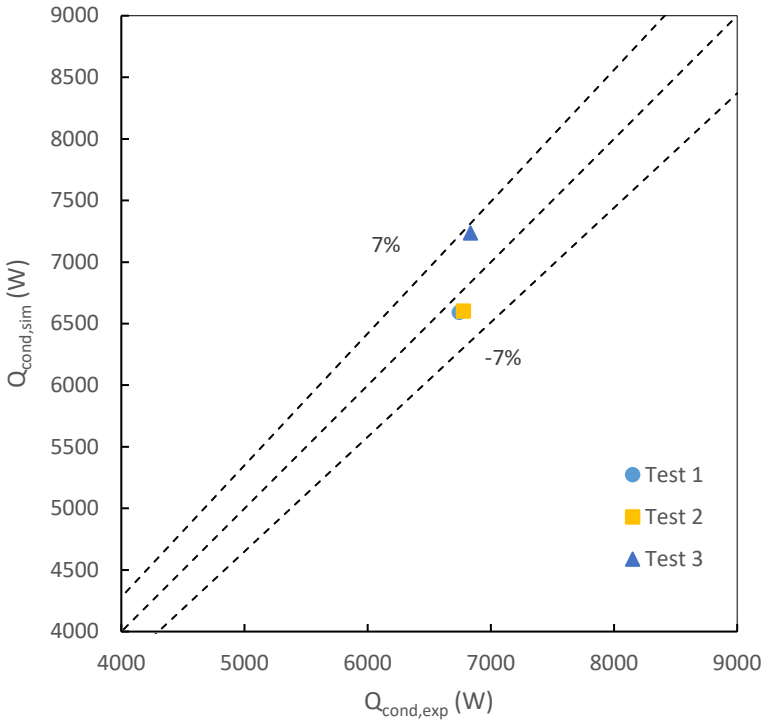

Figure 4-9: Condenser Capacity

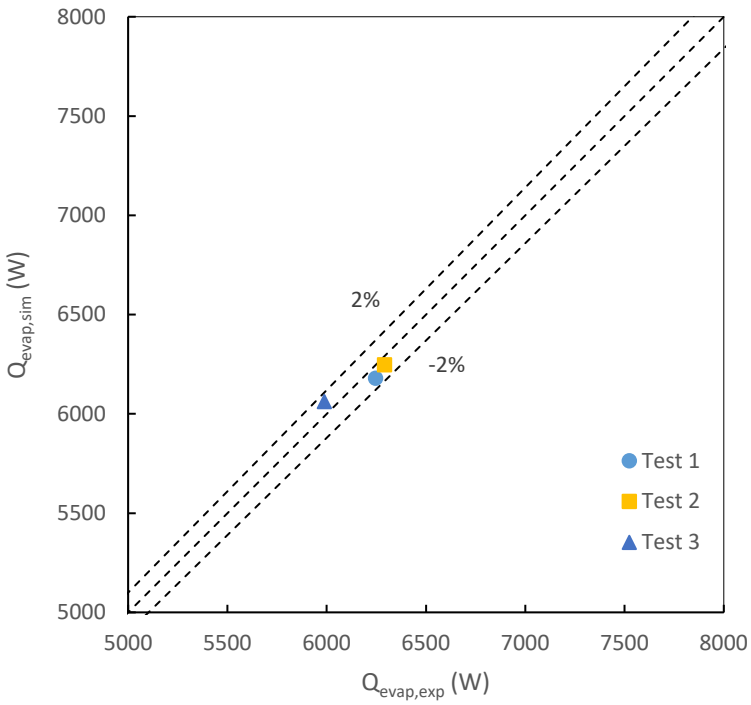

Figure 4-10: Evaporator Capacity

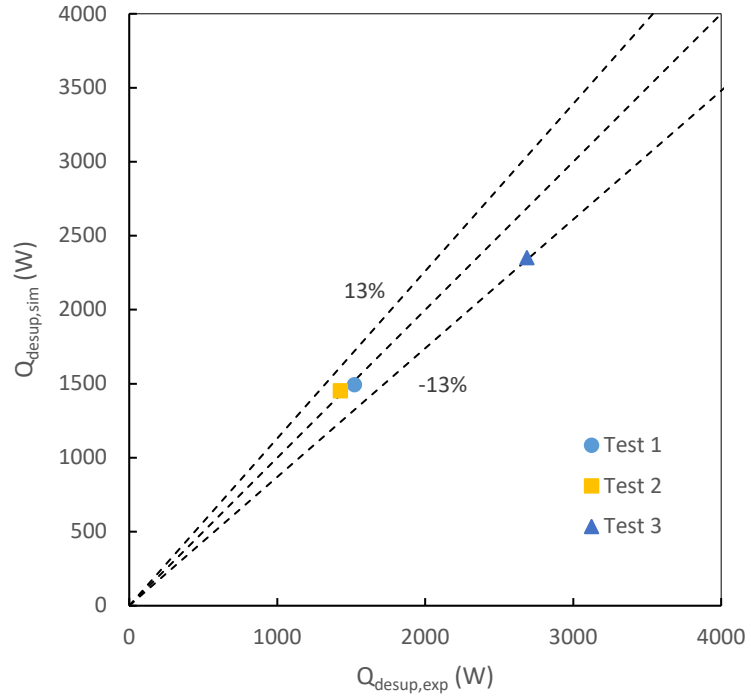

Figure 4-11: Desuperheater Capacity

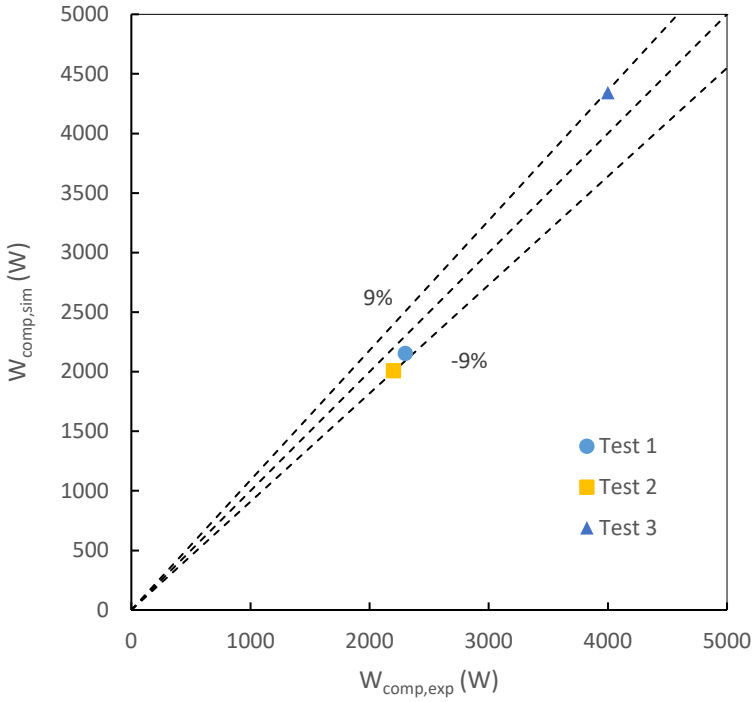

Figure 4-12: Compressor Power

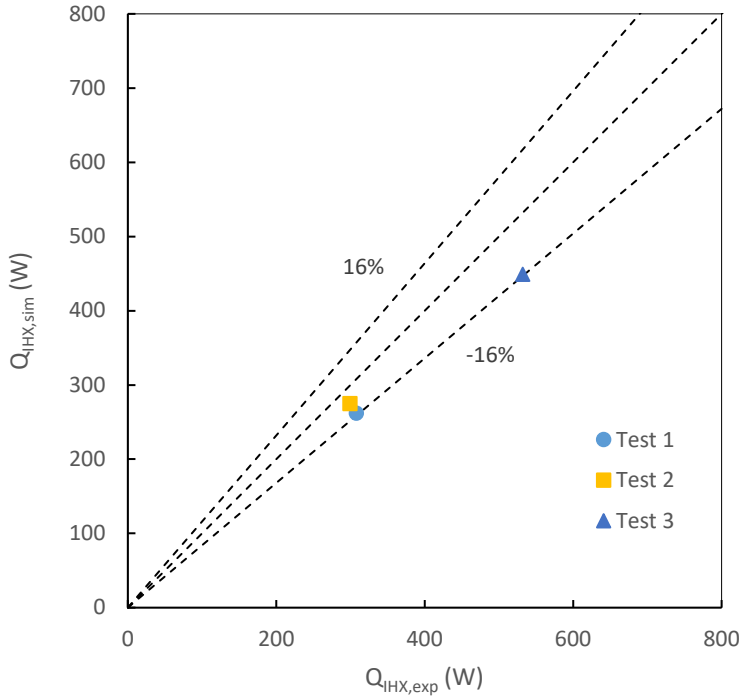

Figure 4-13: Internal Heat Exchanger Capacity

4.2.2 Secondary Loop System

For the SL system, since there is no real system has been built, validation is impossible. The test condition for Test 2 was selected here. And three refrigerants were used when doing simulation for SL system. They were R-134a, R-152a, and R-1234yf. The evaporator outlet superheat and condenser outlet subcooling was fixed at 8°C and -17°C, respectively. Since the evaporator is replaced with an intermediate heat exchanger in SL system, the coolant temperature is much lower than the original air temperature. Therefore, to reach similar capacity as DX system, the evaporating pressure must be lowered. However, this will lead to lower suction density, thus lower mass flow rate. Also, since the evaporating pressure is lower, in order to reach similar capacity while the evaporator outlet superheats is the same, larger refrigerant mass flow rate is required. Therefore, the refrigerant mass flow rate has to be increased in SL system. There are mainly two ways to increase refrigerant mass flow rate in this SL system. One is to increase compressor RPM, the other is to increase the compressor displacement volume. Since the compressor efficiency will suffer a lot when the compressor RPM increases, in order to reach higher refrigerant mass flow rate, a higher displacement volume should be a better choice. As a result, the compressor displacement volume in SL system was increased to $0.00005m^3$, which is around 50% increase, while the compressor RPM remained at 5000. The simulation results are listed on the Table 4-5.

The results show that when maintaining the same superheat for evaporator and same subcooling for the condenser, the capacity of R-1234yf is 5% lower than that of R-134a and R-152a. While the capacity is almost the same, the condensing pressure and evaporating pressure of R-152a are 12.7% and 11.2% lower than that of R-134a, which allows tube with a thinner

thickness to be used in R-152a system to reduce cost. And due to the smaller liquid density of R-152a, compared to the SL system with R-134a, the refrigerant mass flow rate of R-152a system is reduced by 40 %. As a result, the SL system with R-152a has smallest pressure drop and compressor work. For R-1234yf, since the heat of vaporization of R-1234yf is smaller than that other two refrigerants, the larger refrigerant mass flow rate is required to reach similar capacity. In the simulation, 25% refrigerant mass flow rate increase was observed when compare it to SL system with R-134a. However, even with 25% increase in refrigerant mass flow rate, the cooling capacity of R-1234yf is still slightly lower than that of R-134a. Therefore, a compressor with larger displacement volume or higher compressor RPM may be needed to catch the difference.

Overall, R-152a has the highest COP, which is followed by R-134a. While the R-1234yf has the poorest performance. And the COP of all three systems is smaller than that of benchmark system. This is mainly because of the high-pressure ratio caused by high condensing pressure and low evaporating pressure. Take condensing pressure as an example. The coolant flows into the condenser was first cooled by the radiator, which means that the coolant temperature must be higher than the air temperature. In this research, the coolant inlet temperature for the condenser is 9 K higher than the air temperature. The capacity of condenser thus is limited by the small temperature difference despite higher heat transfer coefficient on the coolant side. In order to provide similar cooling capacity, a higher condensing pressure is required. This problem also exists for the evaporator. And as mentioned before, lower suction pressure usually means lower suction density. As a result, the refrigerant mass flow rate will decrease a lot even when the compressor RPM is still the same. Therefore a compressor with larger displacement volume is needed, which leads to the higher power consumption of the compressor. All these factors together are the reasons why the SL system has lower COP.

Table 4-4: Simulation Results of SL Steady-State Model

	R-134a	R-152a	R-1234yf
Q_{cond} [W]	9,196	9,075	8,822
Q_{evap} [W]	6,506	6,539	6,165
W_{comp} [W]	3,380	3,133	3,293
COP	1.92	2.09	1.87
$\dot{m}_{ref}$ [kg/s]	0.04624	0.02787	0.05793
p_{suc} [kPa]	256	236.3	277.1
p_{dis} [kPa]	1811	1581	1787
$p_{cond,in}$ [kPa]	1793	1565	1769
$p_{cond,out}$ [kPa]	1786	1560	1760
$p_{evap,in}$ [kPa]	293	260.4	323.2
$p_{evap,out}$ [kPa]	256	236.3	277.1
T_{suc} [kPa]	4.421	4.918	4.188
T_{dis} [kPa]	92.85	106.8	77.91
$T_{cond,in}$ [kPa]	89.97	103.5	75.49
$T_{cond,out}$ [kPa]	45.48	44.57	46.11
$T_{evap,in}$ [kPa]	0.0036	-0.4155	0.6830
$T_{evap,out}$ [kPa]	4.421	4.918	4.188

5 Transient Simulation

5.1 Modeling Approach

5.1.1 Components

5.1.1.1 Control Volume

The heat exchanger model in Dymola mainly consists of three parts, two fluid control volume, and wall model. Where the fluid control volume can be refrigerant, air or coolant control volume and is fully depended on the real configuration of the heat exchanger. The details of each control volume will be discussed in the following text.

5.1.1.1.1 Refrigerant Control Volume

As the most important control volume in the transient model, the refrigerant control volume has the most complex governing equation and segmentation. For refrigerant-side calculation, finite volume method is used to calculate its thermal performance. For simplicity, the refrigerant flow is assumed to be homogeneous flow. Therefore, the velocity difference between the vapor phase and the liquid phase is zero and the flow-weighted enthalpy is equivalent to the specific enthalpy. Thus the governing equations for each control volume are as follows:

$$V\frac{d\rho}{dt} = \dot{m}_{in} - \dot{m}_{out} \tag{5-1}$$

$$V\left[\rho\frac{dh}{dt} + h\frac{d\rho}{dt} - \frac{dp}{dt}\right] = \dot{m}_{in}h_{in} - \dot{m}_{out}h_{out} - \dot{Q}_w \tag{5-2}$$

$$\Delta z\frac{d\dot{m}}{dt} - \left(\frac{\dot{m}_{in}^2}{\rho A} - \frac{\dot{m}_{out}^2}{\rho A}\right) = -A(p_{out} - p_{in}) - \tau P\Delta z - \rho g V sin\theta \tag{5-3}$$

where Δz is the length of the segment along the flow direction and τ is the wall sheer stress. The first equation is the mass conservation of the control volume. The second equation is the energy conservation and the last equation is the momentum conservation.

Although the time derivative of density can be directly calculated by the Modelica function “der”, the calculation takes relative a long time. To speed up the calculation, the density derivative over time is expanded according to the chain rule:

$$\frac{d\rho}{dt} = \left(\frac{\partial\rho}{\partial p}\right)_h \frac{dp}{dt} + \left(\frac{\partial\rho}{\partial h}\right)_p \frac{dh}{dt} \tag{5-4}$$

After doing so, each term on the right-hand side has a function call associated with it in the refrigerant property library and therefore can be directly calculated, which helps to reduce the calculation time.

For the momentum conservation equation, the left-hand side represents the dynamic pressure waves and are of minor interest in the heat transfer analysis and therefore can be ignored. And since all heat exchanger is horizontally installed, the gravity term can be eliminated from the equation.

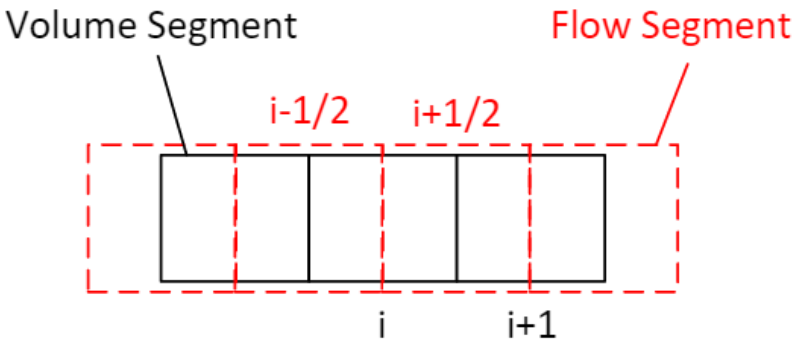

Figure 5-1: Staggered Grid Scheme

Finally, to better solve all three governing equations, the staggered grid scheme is utilized to decouple the momentum conservation equation with mass and energy conservation equation as shown in Figure 5-1. There are two sets of the segment: volume segment and flow segment. Since it is stagger grid scheme, the center of the volume segment is the boundary of flow

segment. The mass and energy balance conservation equations are solved in volume segments while the momentum conservation equation is solved in flow segment.

The final governing equations can then be rearranged as follows:

$$V\left[\left(\frac{\partial \rho_i}{\partial p_i}\right)_h \frac{dp_i}{dt} + \left(\frac{\partial \rho_i}{\partial h_i}\right)_p \frac{dh_i}{dt}\right] = \dot{m}_{i-1/2} - \dot{m}_{i+1/2} \tag{5-5}$$

$$\begin{aligned} V\left[\rho_i \frac{dh_i}{dt} + h_i\left[\left(\frac{\partial \rho_i}{\partial p_i}\right)_h \frac{dp_i}{dt} + \left(\frac{\partial \rho_i}{\partial h_i}\right)_p \frac{dh_i}{dt}\right] - \frac{dp_i}{dt}\right] \\ = \dot{m}_{i-1/2}h_{i-1/2} - \dot{m}_{i+1/2}h_{i+1/2} - Q_w \end{aligned} \tag{5-6}$$

$$0 = -A(p_{i+1} - p_i) - \tau_{i+1/2} P \Delta z \tag{5-7}$$

In the current model, it is difficult to calculate wall shear stress. Therefore, equation (5-7) is replaced with a simpler equation

$$p_{i+1} - p_i = \left(\frac{\dot{m}}{\dot{m}_0}\right)^2 dp_0 \tag{5-8}$$

where $\dot{m}_0$ and dp_0 comes from experimental data.

Since pressure is a necessary input for most function calls of refrigerant property and specific enthalpy can be easily used to calculate the refrigerant quality to determine whether if the current segment is in two-phase state or single-phase state. They are selected as the state variables for the current model.

The specific enthalpy of the volume segment and flow segment satisfy the following equation:

$$h_{i+1/2} = h_i \delta + (1 - \delta) h_{i+1} \tag{5-9}$$

where δ is defined as follows:

$$\delta = \begin{cases} 1 \; when \; \dot{m}_{i+1/2} \geq 0 \\ 0 \; when \; \dot{m}_{i+1/2} < 0 \end{cases} \tag{5-10}$$

Such that

$$h_{i+1/2} = \begin{cases} h_i & when\ \dot{m}_{i+1/2} \geq 0 \\ h_{i+1} & when\ \dot{m}_{i+1/2} < 0 \end{cases} \tag{5-11}$$

And the mass flow rate of both segments satisfy the following equation:

$$\dot{m}_i = \frac{\dot{m}_{i-1/2} + \dot{m}_{i+1/2}}{2} \tag{5-12}$$

The heat transfer coefficient of the refrigerant segment is calculated by the correlations associated with the state of the refrigerant.

For microchannel heat exchanger, the single-phase transfer coefficient is calculated by the Dittus-Boelter correlation [40] which is as follows:

$$Nu = 0.023 Re^{0.8} Pr^{c} \tag{5-13}$$

where c is 0.3 for cooling of the fluid and 0.4 for heating.

For evaporator, the boiling heat transfer coefficient is calculated by the correlation proposed by Yun et al. [41] which is as follows:

$$h = 13678 (Bo \times We_l)^{0.1993} Re_l^{-0.1626} \tag{5-14}$$

where

$$Bo = \frac{q''}{G h_{fg}} \tag{5-15}$$

$$We_l = \frac{G^2 D_h}{\rho_l \sigma} \tag{5-16}$$

$$Re_l = \frac{G(1-x) D_h}{\mu} \tag{5-17}$$

For the condenser, the condensation heat transfer coefficient is calculated by the correlation developed by Shah et al. [42]:

$$h = h_l \left[(1-x)^{0.8} + \frac{3.8x^{0.76}(1-x)^{0.04}}{\mathrm{Pr}^{0.38}} \right] \tag{5-18}$$

where h_l is calculated by the following equation

$$h_l = \frac{k_l}{D_h} 0.023 \left(\frac{G(1-x)D_h}{\mu_l} \right)^{0.8} Pr^{0.3} \tag{5-19}$$

For the compact heat exchanger, the heat transfer correlation is the same as the steady state model and therefore will not be explained for brevity.

5.1.1.1.2 Wall

The tube wall is modeled like lumped capacitances which satisfy the following energy conservation equation

$$\left(Mc_p\right) \frac{dT_W}{dt} = \dot{Q}_{rw} - \dot{Q}_{aw} \tag{5-20}$$

where the left-hand side represents the energy stored in the tube wall and the right-hand side represents the difference between the inlet energy flow and outlet energy flow. The refrigerant side and air side energy flow are calculated as follows

$$\dot{Q}_{rw} = htc_r A(T_r - T_w) \tag{5-21}$$

$$\dot{Q}_{aw} = \dot{m}_a \left[c_{p,a}\left(T_{a,in} - T_{a,out}\right) + \left(\omega_{a,in} - \omega_{a,out}\right)\Delta h_{fg} \right] \tag{5-22}$$

The details of the air side energy flow calculation will be explained in the next section.

5.1.1.1.3 Air Control Volume

For the air side control volume, finite element method is also used. The following assumption is made for the air-side analysis:

1. The air flow is one-dimensional quasi-steady flow
2. Heat conduction in air flow direction is neglected

3. The fin temperature profile is steady-state profile and in each segment, the fin temperature is the same as wall temperature
4. Lewis analogy is valid
5. There is no pressure drop on the air side

The air side governing equations are as follows

$$\dot{m}_a c_{p,a} \frac{dT_a}{dy} \Delta y = \alpha_a (A_{o,t} + \eta_{fin} A_{o,fin})(T_w - T_a) \tag{5-23}$$

$$\dot{m}_a \frac{d\omega_a}{dy} \Delta y = \alpha_m (A_{o,t} + \eta_{fin} A_{o,fin}) \min(0, \omega_{w,s} - \omega_a) \tag{5-24}$$

where Δy is the direction of the air flow, α_m is the mass transfer coefficient is calculated by Lewis analogy

$$\alpha_m = \frac{\alpha_a}{c_{p,a} Le^{2/3}} \tag{5-25}$$

where the Le is Lewis number and it is equal to 1 for this model.

Solving equation (5-21) and (5-22) yields

$$T_{a,out} = T_{a,in} + (T_w - T_{a,in}) \left\{ 1 - \exp \left[- \frac{\alpha_a (A_{o,t} + \eta_{fin} A_{fin})}{\dot{m}_a c_{p,a}} \right] \right\} \tag{5-26}$$

$$\omega_{a,out} = \omega_{a,in} + min(0, \omega_{w,s} - \omega_a) \left\{ 1 - exp \left[- \frac{\alpha_m (A_{o,t} + \eta_{fin} A_{fin})}{\dot{m}_a} \right] \right\} \tag{5-27}$$

Thus the air side outlet condition can be calculated by the air inlet condition. Then, the air side capacity can be calculated using equation (5-22). While the first term on the right-hand side of equation (5-22) is the sensible load and the second term on the right-hand side is the latent load. And the condensate water is obtained by dividing the latent load over the heat of vaporization of water:

$$\dot{m}_{water} = \frac{Q_{latent}}{\Delta h_{fg}} \tag{5-28}$$

The fin efficiency is defined as:

$$\eta_f = \frac{\tanh(mL)}{mL} \tag{5-29}$$

$$m^2 = \frac{2\alpha}{k_f \delta_f} \tag{5-30}$$

$$L = \frac{H_f}{2} \tag{5-31}$$

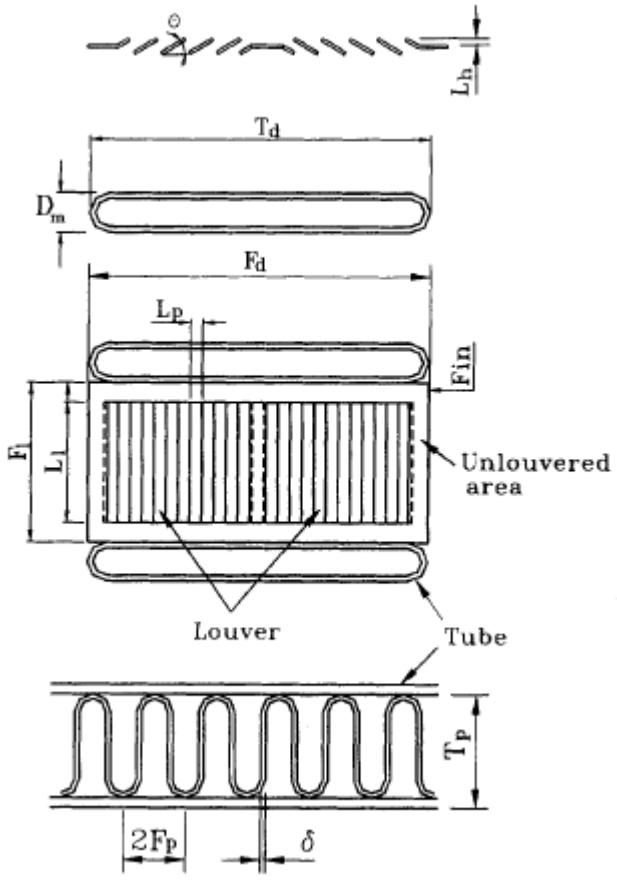

Figure 5-2: Definition of Louver Fin Geometry Parameters [43]

The correlation proposed by Wang et al. [43] is utilized to calculate the air side heat transfer coefficient for louver fin (Figure 5-2)

$$j = Re^{-0.49}\left(\frac{2\theta}{\pi}\right)^{0.27}\left(\frac{F_p}{L_p}\right)^{-0.14}\left(\frac{F_l}{L_p}\right)^{-0.29}\left(\frac{T_d}{L_p}\right)^{-0.23}\left(\frac{L_l}{L_p}\right)^{0.68}\left(\frac{T_p}{L_p}\right)^{-0.28}\left(\frac{\delta_f}{L_p}\right)^{-0.05} \quad (5\text{-}32)$$

where θ is louver angle, F_p is fin pitch, L_p is louver pitch, F_l is fin length, T_d is tube depth, L_l is louver length, T_p is tube pitch.

5.1.1.1.4 Coolant Control Volume

The same as other control volumes, finite volume method is utilized in the coolant side control volume. Since the ethylene glycol-water mixture property doesn't consider pressure as an input for the most function call, the pressure drop on the coolant side is ignored for simplicity. Thus, only energy and mass conservation equations need to be solved and there is no need to use staggered-grid scheme. And due to the simplicity of the water\ethylene glycol library, one cannot directly call time derivative of density. Therefore, a simplified set of conservation equation is used on coolant side control volume, which is as follows:

$$\dot{m}_{in} = \dot{m}_{out} \quad (5\text{-}33)$$

$$\dot{m}c_{p,eg}\frac{dT}{dt} = \dot{m}_{in}h_{in} - \dot{m}_{out}h_{out} - Q_w \quad (5\text{-}34)$$

Since the coolant flow is always single-phase in this research, the Dittus-Boelter correlation for single-phase heat transfer is used in the coolant control volume.

5.1.1.1.5 Lumped Control Volume

Lumped control volume is the control volume used in each auxiliary component which determines the change of the refrigerant state inside the component. The governing equations for the lumped control volume are similar to the heat exchange refrigerant side governing equations and the only difference is that the lumped control volume only has one segment and the pressure drop is neglected in the lumped control volume. Therefore the momentum conservation equation

is not included in the governing equations for this control volume. The mass and energy balance equations are equation (5-5) and equation (5-6), respectively.

5.1.1.2 Microchannel Heat Exchanger

The microchannel heat exchanger consists of three parts: refrigerant control volume, air control volume and wall models. The refrigerant is assumed to be evenly distributed in each tube. Therefore, the whole pass can be solved by solving one tube. The details of each control volume have been introduced in the previous section about the control volume and will not be discussed here for brevity.

Table 5-1: Evaporator Test Condition

Test Number	Test 1	Test 2	Test 3	Test 4
$T_{a,in}$ [°C]	27	27	27	27
$RH_{a,in}$ [%]	50	50	50	50
$VFR_{a,in}$ $[m^3/s]$	0.056	0.083	0.111	0.139

Table 5-2: Condenser Test Condition

Test Number	Test 1	Test 2	Test 3	Test 4
$T_{a,in}$ [°C]	37	37	37	37
$VFR_{a,in}$ $[m^3/s]$	0.405	0.607	0.809	1.012

The microchannel heat exchanger serves as condenser and evaporator in DX system. The condenser and evaporator models were validated by the experimental data. The test condition of evaporator and condenser are listed in Table 5-1 and Table 5-2.

The comparison between the simulation results and experimental data is listed in Figure 5-3 and Figure 5-4. The deviation of evaporator capacity and condenser capacity are less than 7% for both models. And the deviation tends to decrease as the air velocity increases. And in general, the evaporator model shows larger deviation than condenser model. This is because the

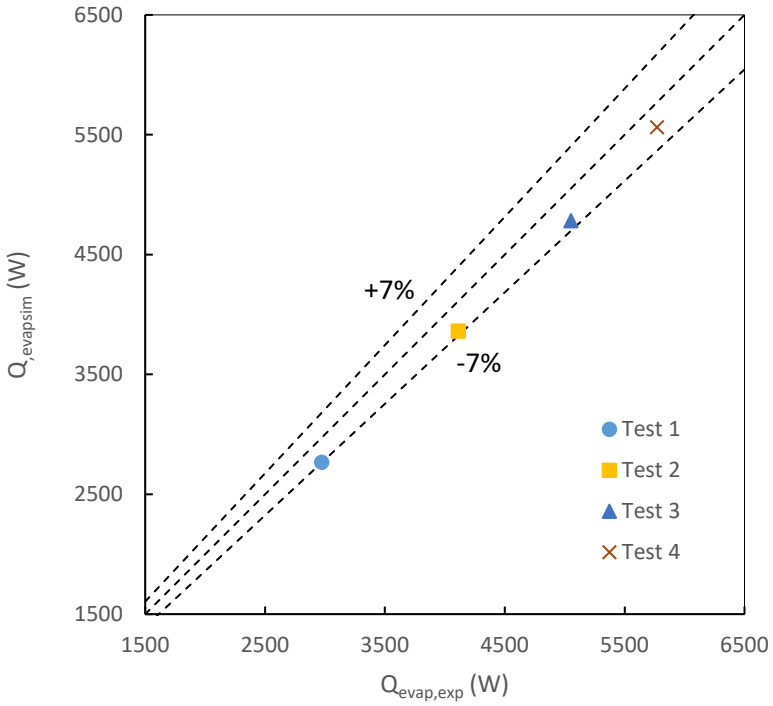

Figure 5-3: Evaporator Validation

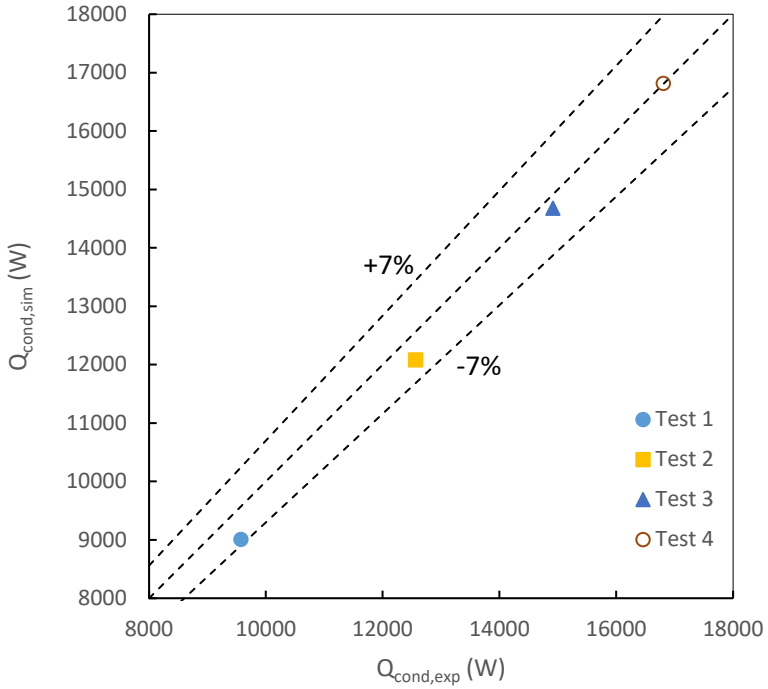

Figure 5-4: Condenser Validation

evaporator has two banks while the condenser only has one. Therefore the deviation of air outlet temperature of the first bank will affect the calculation in the second bank, which leads to the augmentation of the deviation.

5.1.1.3 Internal Heat Exchanger

For simplicity, the heat loss to the ambient is neglected. Therefore only three components are necessary for the internal heat exchanger model, which are two refrigerant control volume and one wall model. The geometry and heat transfer coefficient calculation of the internal heat exchanger model is the same as the model approach used in the steady-state model which has been discussed before therefore is skipped here for brevity. The pressure drop correlation is not used due to chattering problem. Instead, the pressure drop is calculated by the equation (5-8).

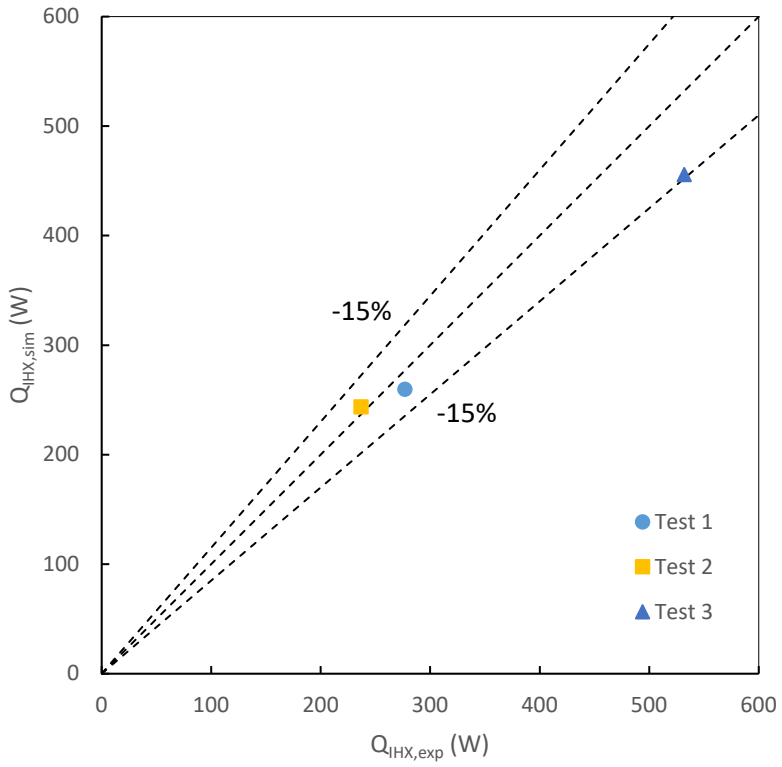

Figure 5-5: IHX Validation

The validation of the internal heat exchanger model is shown in Figure 5-5. Test 1 and Test 2 shares same refrigerant mass flow rate, while the refrigerant mass flow rate of test 3 increases by 8%. And high-pressure side inlet temperature of Test 3 is 10 K higher than that of Test 1 and Test 2. The result shows that the deviation of internal heat exchanger capacity is within 15%. The Larger deviation is observed in Test 3. This is because the heat loss to the ambient is neglected in this model and the temperature of the high-pressure side for Test 3 is much higher than that of other two test conditions.

5.1.1.4 Compact Heat Exchanger

For compact heat exchanger, the air side control volume of the microchannel heat exchanger is replaced with coolant control volume. And refrigerant side calculation is also shifted from microchannel to offset strip fin. The details of the calculation of geometry parameters and the heat transfer coefficient have been discussed in the previous chapter and therefore are skipped here for brevity.

5.1.1.5 Compressor

The compressor model is considered as in quasi-steady state and is an efficiency-based model. The mathematic description is the same as the steady-state model. Therefore the details of the compressor base model are skipped here for brevity.

5.1.1.6 Expansion Valve

A simple orifice model is used as the expansion device. The governing equation for this model is:

$$\dot{m} = C_v A \sqrt{\rho_{in} \Delta p} \tag{5-35}$$

where C_v is the flow coefficient of the valve and is obtained by the experimental data.

5.1.1.7 Receiver

The receiver is modeled as a tank with both liquid and vapor refrigerant inside. The inlet refrigerant is in two-phase and the outlet refrigerant is always liquid-phase.

The following assumption is made to build the receiver model:

1. Ideal phase separation
2. Vapor and liquid inside the receiver are in thermodynamic equilibrium
3. No pressure drop between the receiver inlet and outlet

The governing equation of the receiver are as follows

$$V\frac{d\rho}{dt} = \dot{m}_{in} - \dot{m}_{out} \tag{5-36}$$

$$V\left[\rho\frac{dh}{dt} - \frac{dp}{dt} + h\frac{d\rho}{dt}\right] = \dot{m}_{in}h_{in} - \dot{m}_{out}h_{out} - \dot{Q}_w \tag{5-37}$$

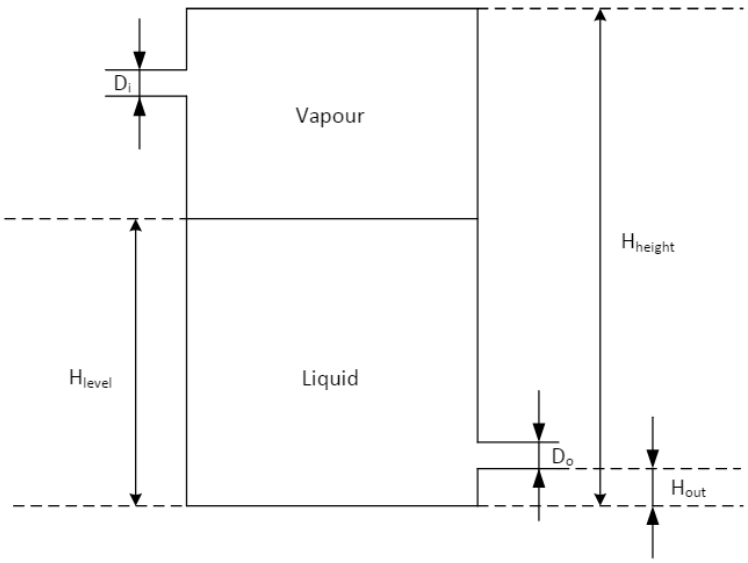

Figure 5-6: Definition of Receiver Parameters

The specific enthalpy calculated by the governing equation can then be used to calculate the refrigerant density. The refrigerant quality inside the receiver is calculated as follows:

$$x = \frac{h - h_l}{h_v - h_l} \tag{5-38}$$

Then the mass of refrigerant vapor is defined by the following equation:

$$M_v = xM_{total} \tag{5-39}$$

$$M_{total} = \rho V \tag{5-40}$$

Then the liquid mass can be calculated by subtracting the total mass by the vapor mass. And the liquid mass is a function of the liquid level inside the receiver:

$$M_l = V \frac{H_{level}}{H_{height}} \max(\rho, \rho_l) \tag{5-41}$$

$$H_{level} = \frac{\rho(1 - x)}{\max(\rho, \rho_l)} H_{height} \tag{5-42}$$

where ρ_l is the refrigerant density of saturated liquid.

It is not difficult to find that the receiver will always full if the inlet refrigerant is in subcooling. The specific outlet enthalpy is then determined by the following equation:

$$h_{out} = \begin{cases} \min(h, h_l) & when\ H_{level} > H_o + D_o \\ h_v + \dfrac{H_{level} - H_{out}}{D_o} & when\ H_o + D_o \geq\ H_{level} \geq H_o \\ \max(h, h_v) & when\ H_{level} < H_o \end{cases} \tag{5-43}$$

5.1.1.8 Cabin

The following assumption is made to develop the cabin model:

1. The properties of air and mass are spatially uniform.
2. The temperature difference between the cabin air and components is small and therefore the radiation of components can be ignored.
3. The solar load is constant.
4. The thermal insulation of the floor and trunk is very good and therefore the heat transfer from those parts can be neglected.

5. The air side pressure drop is neglected

The governing equations for the cabin are as follows:

$$M_r c_{p,r} \frac{dT_r}{dt} + M_c c_{p,c} \frac{dT_c}{dt} = \frac{\dot{m}_{in}(c_{p,in} + c_{p,out})}{2}(T_s - T_r) + \dot{Q}_{sol} + \dot{Q}_{ps} + U_o A_o (T_{amb} - T_r) + \dot{m}_{iv} c_{pamb} (T_{amb} - T_r) \quad (5\text{-}44)$$

$$M_c c_{pc} \frac{dT_c}{dt} = -h_c A_c (T_c - T_r) \quad (5\text{-}45)$$

$$M_r h_{fg,r} \frac{d\omega_r}{dt} = (\dot{m}_{water,s} + \dot{m}_{water,o} + \dot{m}_{water,infil}) \frac{h_{fg,r} + h_{fg,s}}{2} + \dot{Q}_{plt} \quad (5\text{-}46)$$

Recirculation of the cabin air is also considered in the model. The return air from the cabin is mixed with the ambient air and then is then sent to the evaporator. The recirculation rate is considered constant for the whole process.

The cabin model was validated with the results of Huang [44]. The inputs for the cabin model are listed in Table 5-6. And the simulation result was compared to that of Huang in Figure 5-4.

Table 5-3: Cabin Model Validation Parameters

Parameters	Values
Passengers	0
Internal Volume [m^3]	8
Collective Mass [kg]	200
Internal HT area [m^2]	3
Outer HT area [m^2]	14.9
Solar Radiation [W]	950
Cabin Initial Temperature [°C]	43.3
Soak Temperature [°C]	16.7

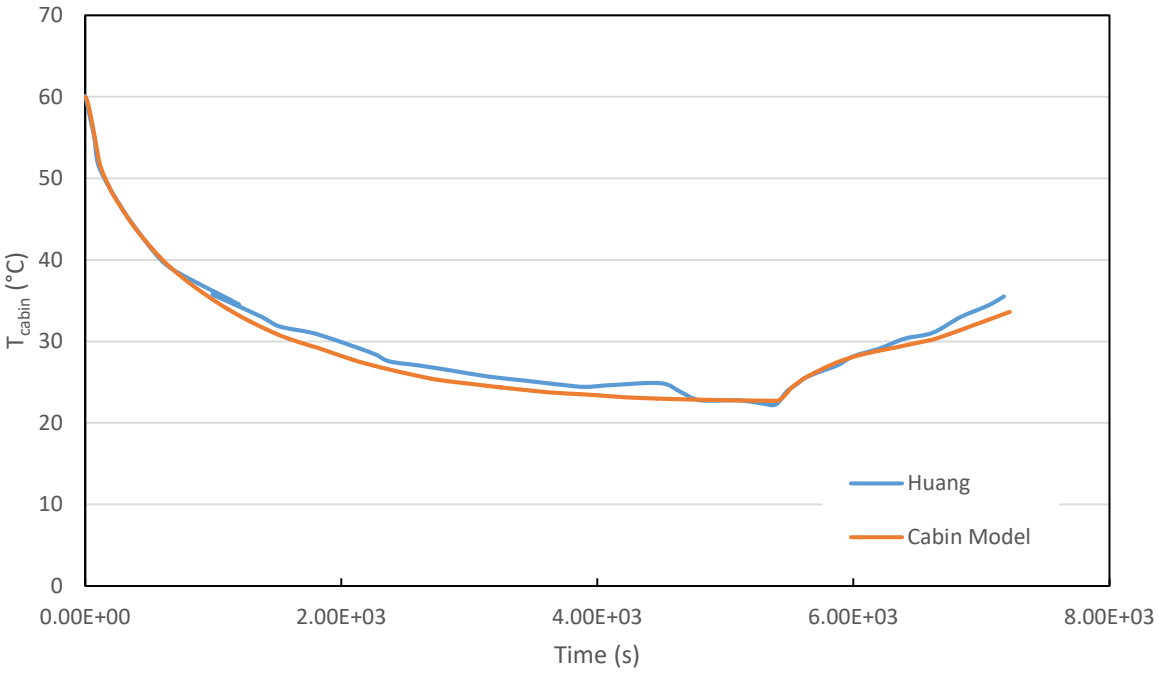

Figure 5-7: Cabin Model Validation

5.1.2 Systems

5.1.2.1 Transient Model for DX System

Each component in Dymola was built with several fluid connectors. Each fluid connector stores the mass flow rate, enthalpy flow rate and pressure of the fluid. Once two flow points are connected, built in mass, energy and momentum conservation equations will be created. Therefore the fluid information can be passed from one component to the next. The system model can then be constructed by connecting ports of each component. To simplify the system model and increase calculation speed, the air inlet state for both condenser and evaporator are passed to the heat exchanger by using an air port model, where the air velocity, temperature, and relative humidity are defined. The final diagram of DX system is displayed in Figure 5-8.

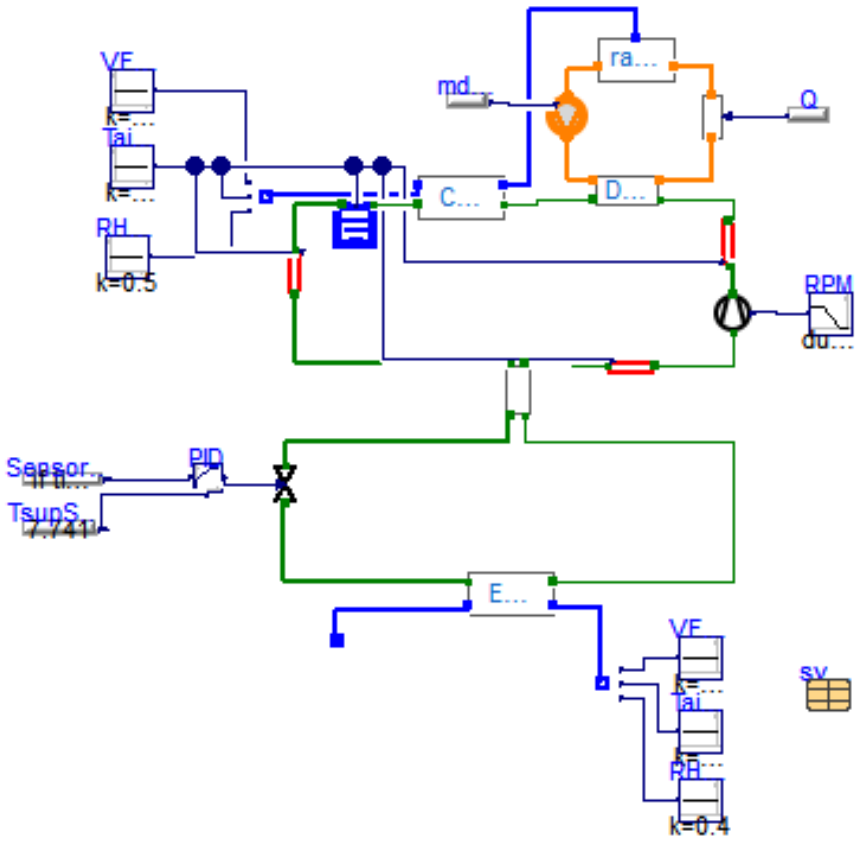

Figure 5-8: Diagram of DX System Model

5.1.2.2 Transient Model for SL System

Similar to the DX system model, the components are connected through connections between fluid ports. And the air inlet state for the condenser is given by the air port model. For cabin cooler, instead of air port model, it is connected with the cabin model. Therefore the SL system model can predict the cabin air temperature change versus time. The final diagram of SL system is displayed in Figure 5-9.

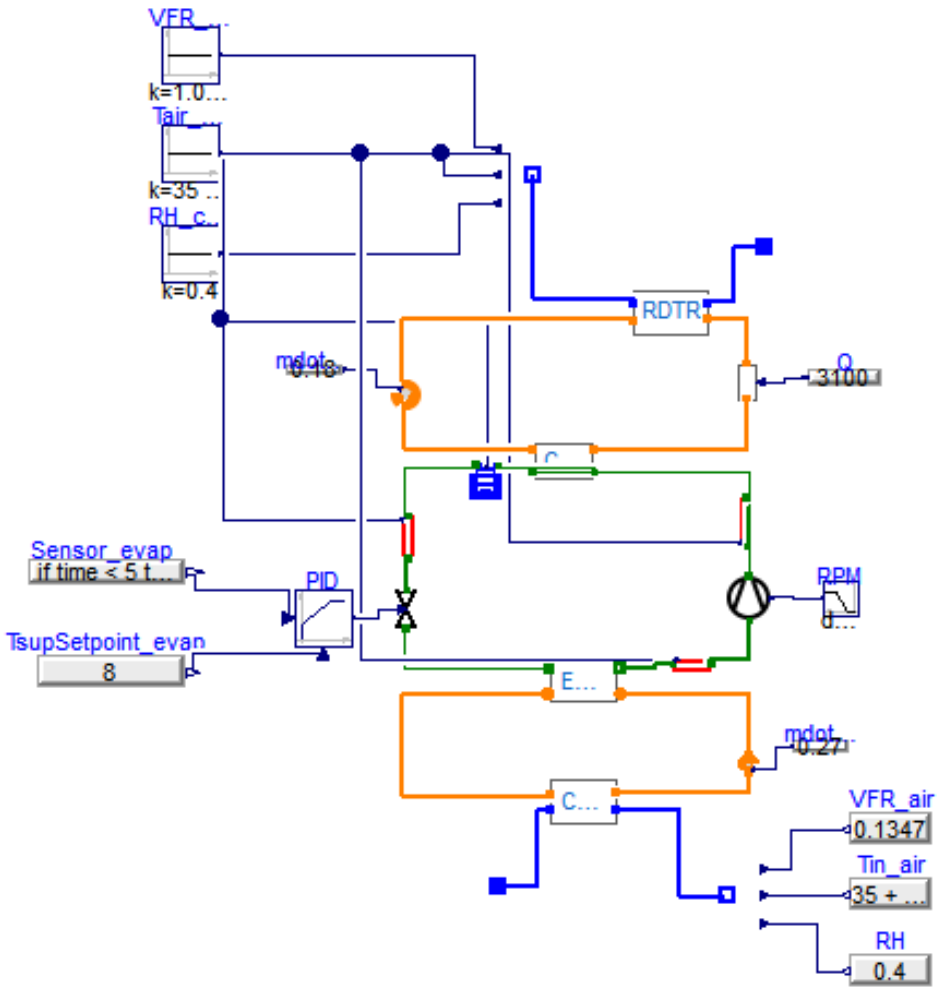

Figure 5-9: Diagram of SL System Model

5.2 Validation of DX System Model

The transient model of DX system was validated by the steady-state experimental data of DX system since that is the only experimental data I have.

All inputs of the transient model were constants. The constant inputs of the transient model are the same as the inputs of the steady-state model and are listed in Table 4-1. By using constant inputs, the transient model will reach steady-state eventually as long as the simulation

time is long enough. Therefore the simulation time was set to be 1,000 seconds with an interval of 1 second. And the built-in Dassl algorithm was used.

The simulation results are shown in Figure 5-10 through Figure 5-14. Condenser, evaporator and desuperheater model show good accuracy with a deviation of capacity less than 2%. Similar to steady-state model in EES, the large deviation was observed for the internal heat exchanger, which is between 2 – 8%. It is mainly caused by simplified geometry and neglecting of the heat loss. Overall the transient model shows good accuracy in terms of capacities and COP.

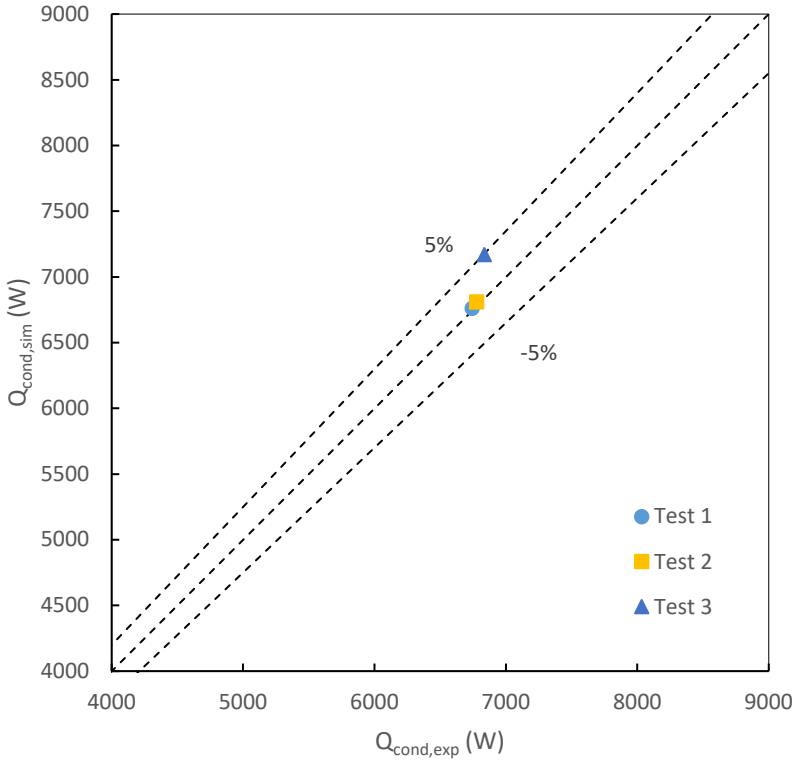

Figure 5-10: Condenser Capacity

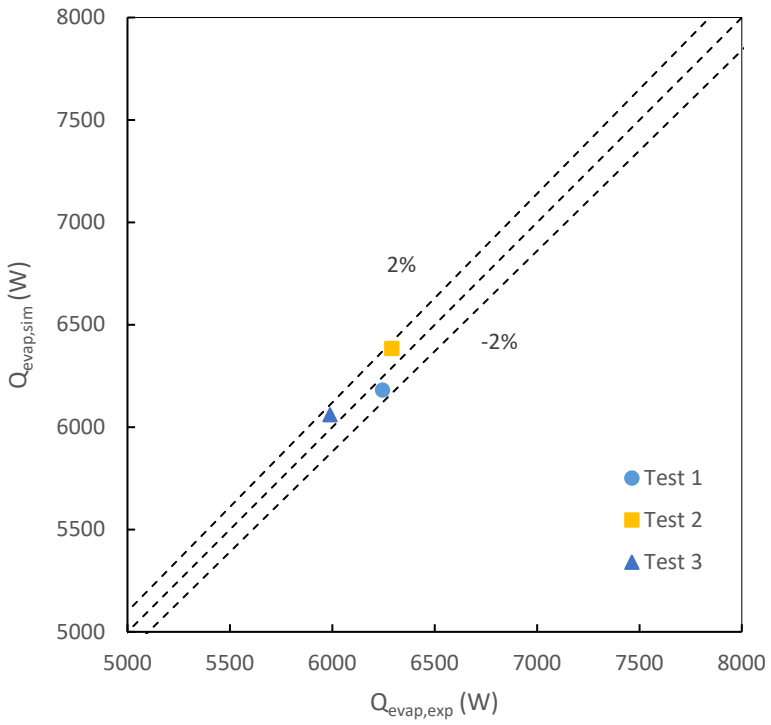

Figure 5-11: Evaporator Capacity

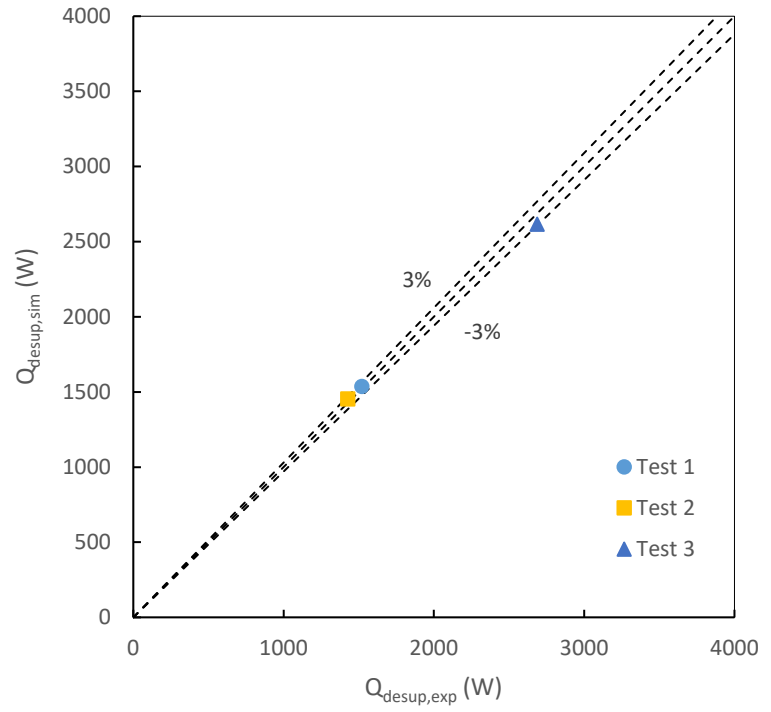

Figure 5-12: Desuperheater Capacity

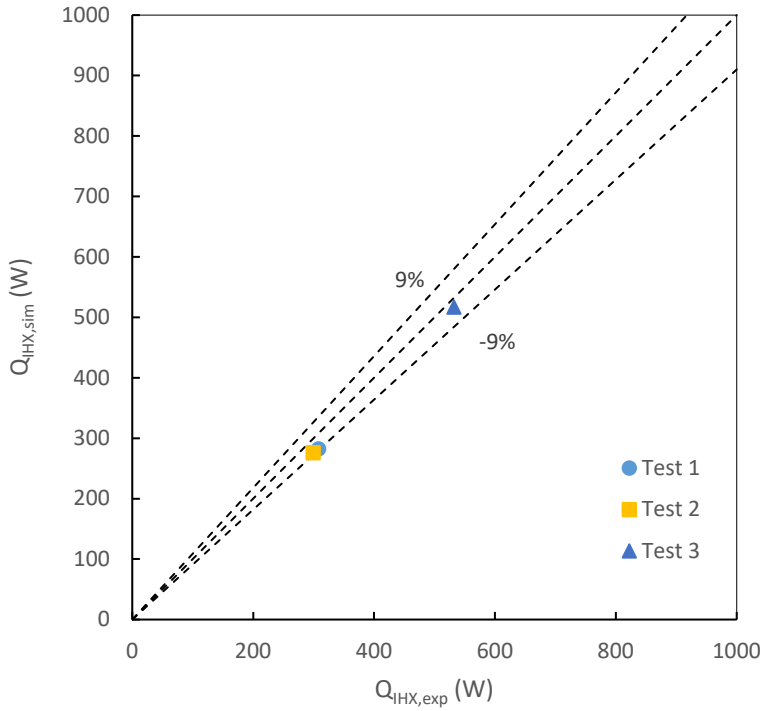

Figure 5-13: Internal Heat Exchanger Capacity

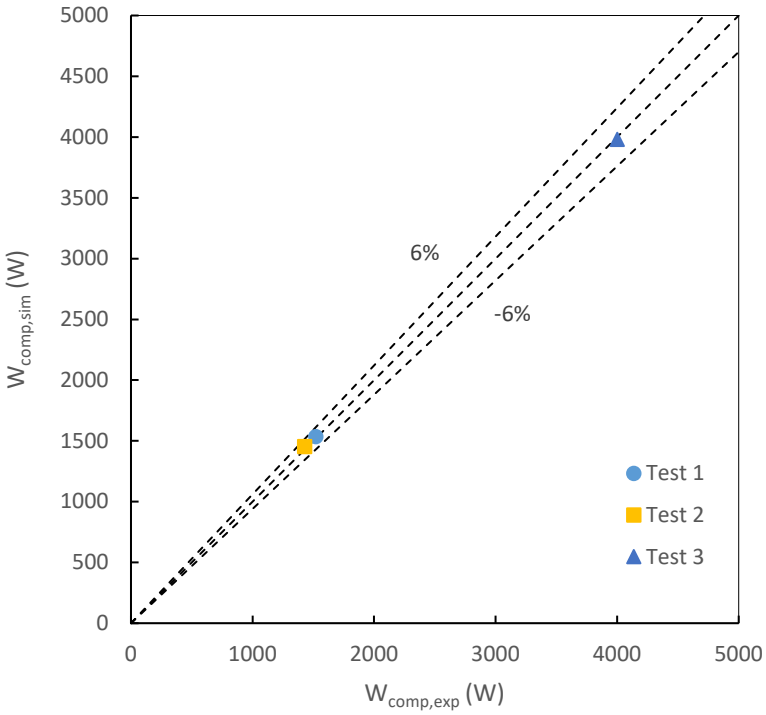

Figure 5-14: Compressor Power

5.3 Transient Simulation Input

US06 supplemental federal test procedure (Figure 5-15) representing aggressive driving behavior with high average speed and rapid speed fluctuations [45] was selected as the driving cycle used in this research. The air inlet velocity for condenser or radiator is interpolated by using the velocity profile. The ambient temperature is set to be 35°C and the relative humidity is 50%. The detailed cabin parameters are shown in Table 5-4. The room temperature is the same as the ambient temperature and the soak temperature is set to be 0°C. The solar radiation is constant at 1,000 W/m^2.

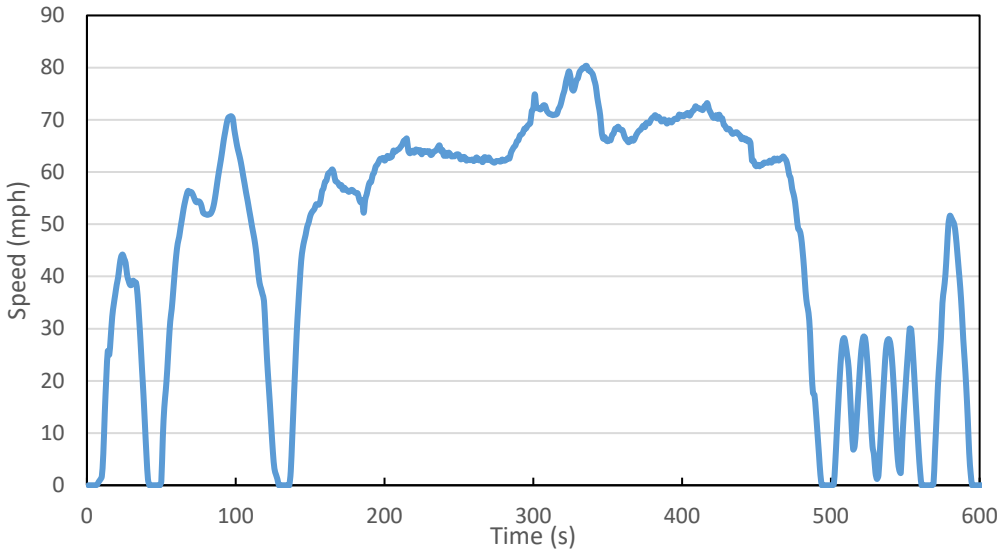

Figure 5-15: US06 Driving Cycle Velocity Profile [45]

Table 5-4: Cabin Parameters

Parameter	Values
Passenger	0
Internal Volume [m^3]	2.4
Collective Mass [kg]	150
Internal HT area [m^2]	3
Outer HT area [m^2]	14.9
Solar Radiation [W]	1000
Cabin Initial Temperature [°C]	35
Soak Temperature [°C]	0
Recirculation Rate [-]	0.05

5.4 Simulation Results

Simulation results of SL system with R-134a, R-152a, and R-1234yf are compared to the results of DX system using R-134a and are shown in Figure 5-16 through Figure 5-19. All the SL systems share the same trend. Figure 5-16 shows the comparison of evaporator capacity. Since the evaporator in SL system is not directly affected by the change of vehicle speed, its capacity is relatively stable during the whole process despite the fluctuation of the car velocity. The capacity curve of R-134a and R-152a SL systems are almost the same, which is slightly lower than that of R-134a DX system. While the R-1234yf system has the lowest cooling capacity.

Figure 5-17 shows the comparison of condenser capacity. It was observed that when the condenser air inlet velocity decreased, the compressor discharge pressure would increase, which lead to higher condenser capacity. And for the DX system, the condenser is directly cooled by the ambient air. Therefore, its capacity shows larger fluctuation compare to the SL system. And since in the DX system, the refrigerant superheat region is cooled by the desuperheater, the capacity of the condenser in DX system is around 2,000 W smaller than that of SL system.

As shown in Figure 5-18, the compressor work of the SL system is much higher than that of DX system, which is similar to the results from the steady-state model. The reasons were discussed in the previous chapter and therefore will not be shown here. The trend of compressor work of all models is almost identical, which is opposite of the vehicle speed. The inlet air velocity decreases as the vehicle slows down, which leads to high discharge pressure and low compressor efficiency. This explains the reason why the compressor work increased when the vehicle speed decreased.

The refrigerant charges of SL systems were also calculated. The refrigerant charges of R-134a SL, R-152a SL and R-1234yf SL are 239 g, 188 g, and 281 g, respectively, which are significantly lower than 497 g charge of R-134a in DX system.

Since the US06 driving cycle only lasts for 600 seconds, the cabin air temperature is still relatively high. As shown in Figure 5-19, the response of R-134a DX system is faster than the SL system. This is because, for the SL system, the air conditioning system needs to cool the coolant first. Only when the coolant is cold enough then the air temperature can be cooled.

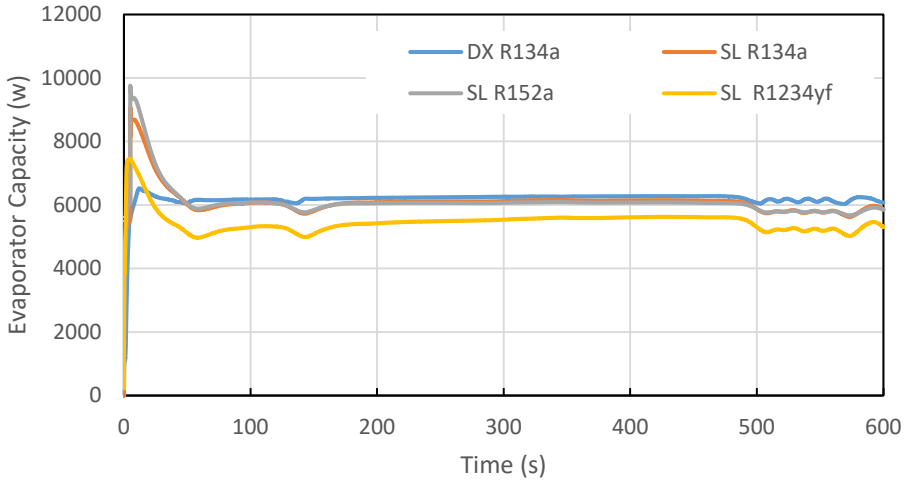

Figure 5-16: Evaporator Capacity Comparison

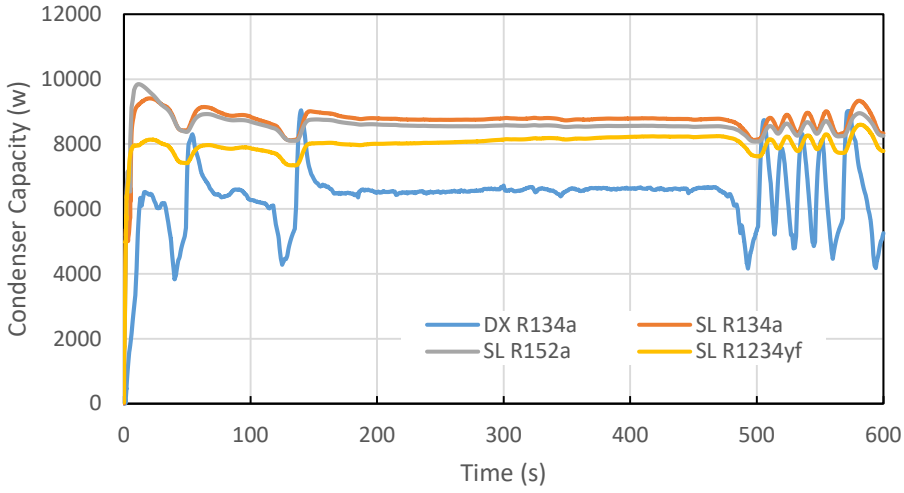

Figure 5-17: Condenser Capacity Comparison

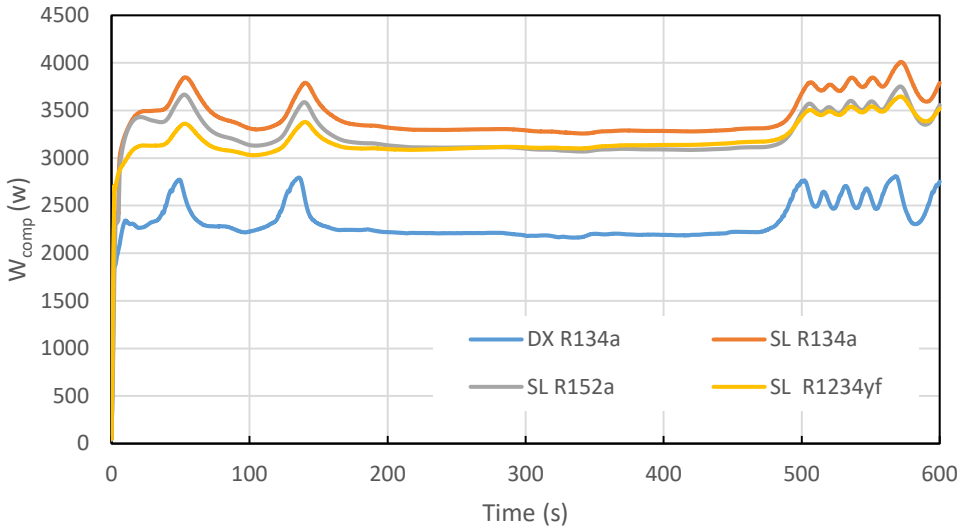

Figure 5-18: Compressor Work Comparison

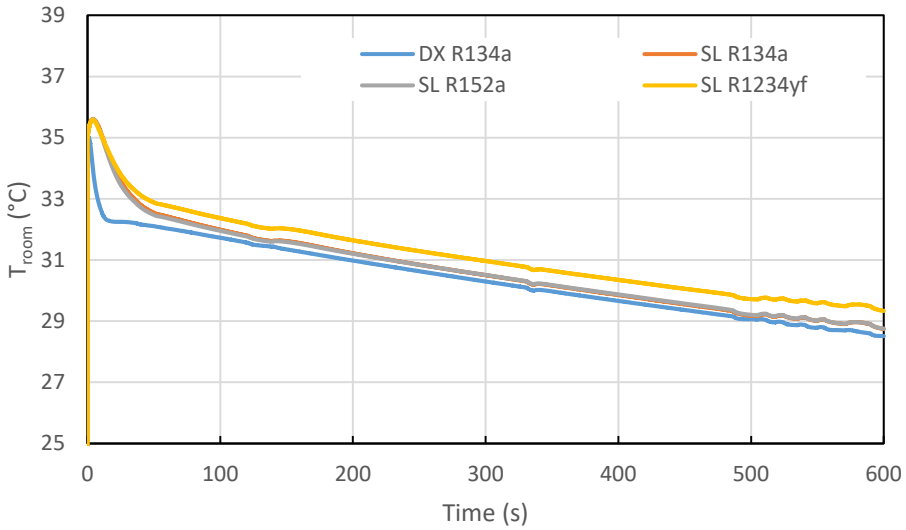

Figure 5-19: Cabin Air Temperature Comparison

5.5 Start/Stop Operation

Due to the large specific heat capacity of ethylene glycol, the coolant inside the secondary loop makes a significant contribution to the system thermal mass. One potential application is to ease the supply air fluctuation during the start/stop operation.

For a vehicle installed with the start/stop system, the engine will stop when the vehicle is completely stopped to reduce fuel consumption. The engine will be started again in a brief time when the driver steps on the gas. Because most conventional MACs are driven by the belt which connects the compressor and engine, the start/stop operation has significant negative effect on their cooling performance.

Due to the fact that the systems studied in this research are driven by the electric compressor, which is independent of the driving condition, the start/stop operation actually has almost no impact on the MACs operation. However, the air flow passing through the condenser is relatively small when the vehicle is stopped, which could cause high condensing pressure and temperature and may harm the system. In addition, turning off the compressor can save the energy and thus potentially increase the energy efficiency of the system. Therefore, it is worth studying what would happen if the compressor were turned off during completely stop.

Since zero refrigerant mass flow rate may cause the singularity in the model, 100 rpm was selected as the minimum compressor revolution speed. The compressor revolution speed profile was reconfigured so that it keeps running at 5,000 rpm at most of the time while turns to 100 rpm when the vehicle is stopped. All other inputs of the model are the same as the inputs discussed in 5.3. In this simulation, direct expansion system running R-134a and secondary loop system running R-134a, R-152a, and R-1234yf were simulated and compared.

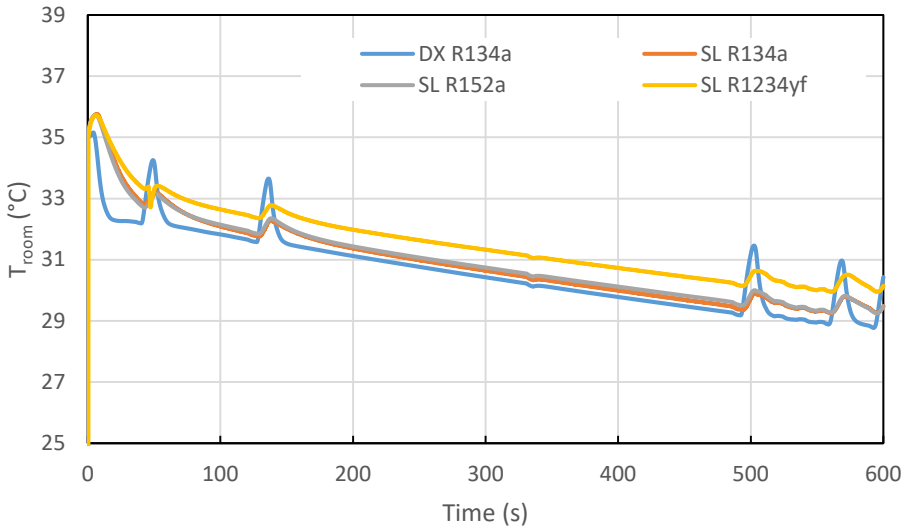

Figure 5-20: Cabin Room Temperature with Start/Stop Operation

When the compressor was shut down, the refrigerant mass flow rate fell towards zero. As a result, the evaporator capacity dropped dramatically, which led to a sharp increase in the supply air temperature and relative humidity as shown in Figure 5-20. For secondary loop system, since the cooling capacity can be stored in the coolant, though the temperature increase still existed, the maximum temperature increase of cabin air was reduced by 75%.

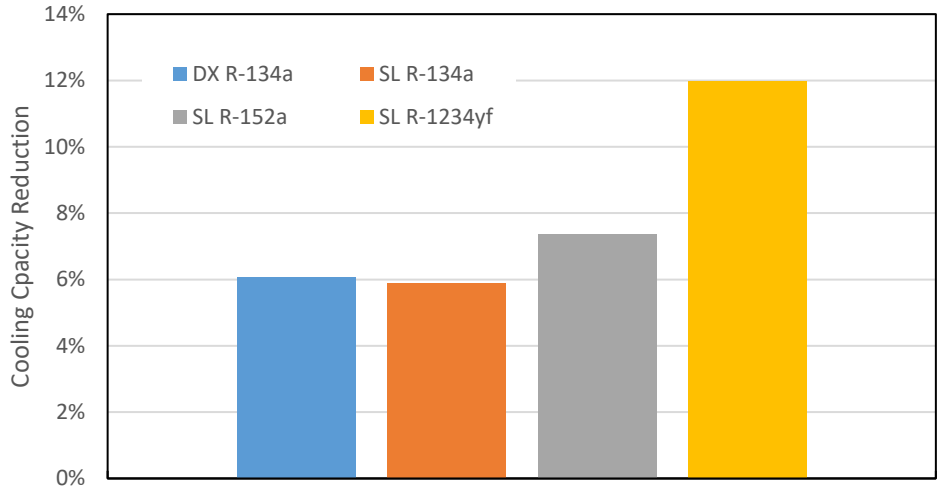

Figure 5-21: Cooling Capacity Reduction Compared to Model without Start/Stop Operation

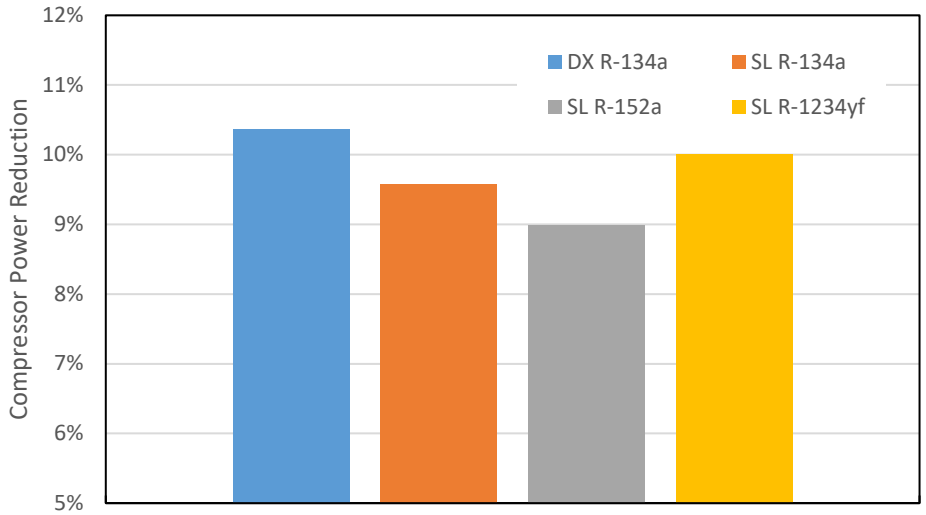

Figure 5-22: Compressor Power Reduction Compared to Model without Start/Stop Operation

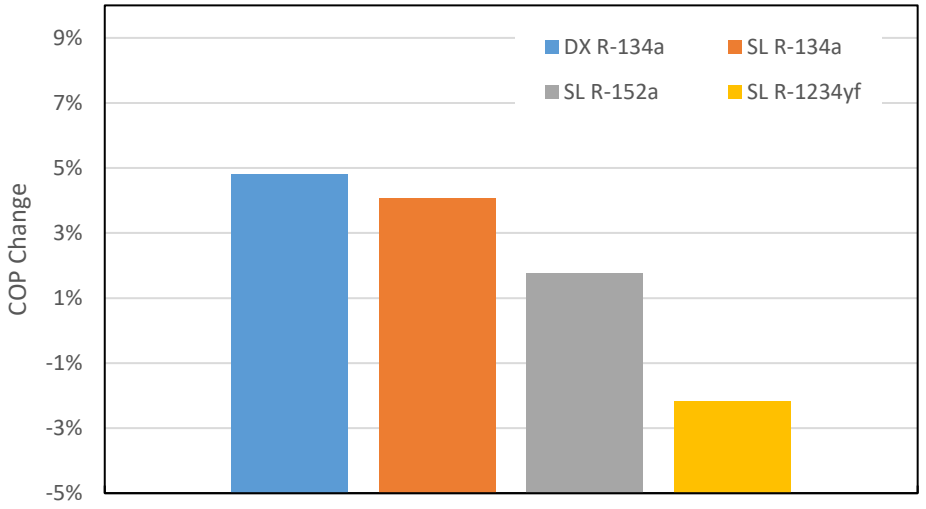

Figure 5-23: COP Change Compared to Model without Start/Stop Operation

Eventually, both accumulated cooling capacity and compressor work reduced for all models as shown in Figure 5-21 and Figure 5-22. For DX R-134a, the accumulated cooling capacity reduced by 6.0%. For secondary loop system, the cooling capacity reduced 5.8%, 7.4% and 12.0% for R-134a, R-152a and R-1234yf, respectively. The compressor power reductions for DX R-134a, SL R-134a, SL R-152a and SL R-1234yf are 10.3%, 9.6%, 9.0% and 10.0%,

respectively. The comparison of COP is shown in Figure 5-23. Since the capacity reduction of SL R-1234yf is more significant than compressor power reduction, the COP of SL R1234yf decreased by 2.2%. While the COP of other models increased 1.8%-5%.

Overall, the start/stop operation increases the system COP by sacrificing cooling capacity. Though the direct expansion system can benefit more from the start/stop operation, the thermal comfort of the direct expansion system would be poorer than that of SL system due to large temperature fluctuation. For SL R-152a, the start/stop operation is a good approach to improve the energy efficiency. While for SL R-1234yf, the start/stop operation should not be used since both cooling capacity and COP will decrease.

6 Life Cycle Climate Performance Comparison

The Life Cycle Climate Performance (LCCP) is a method used to evaluate the global warming impact of the air conditioning system from the cradle to the grave. It considers both direct and indirect emissions. The direct emission accounts for the emission from the leakage of the air conditioning system throughout its lifetime, while the indirect emission accounts for the emission from energy consumption, unit and refrigerant manufacturing process as well as the disposal of the air conditioning system.

The direct emission is calculated [46] by

$$Direct\ Emission = [C \times (L \times ALR) + EOL] \times (GWP + Adp.GWP) \quad (6\text{-}1)$$

where C is the charge of refrigerant, $Adp.GWP$ is the Global Warming Potential of Atmosphere Degradation Product of the refrigerant, L is the average Lifetime of equipment, ALR is the Annual Leakage Rate, and EOL is the End of Life emissions.

Due to the complex traffic and road condition, when calculating the ALR, in addition to the 6.9 %/yr regular leakage [47], irregular leakage caused by small incidents and maintenance services should be included as well, which are 20 g per year and 60 g per service, respectively [48]. And similar to the residential air conditioning system, the EOL of MAC is assumed to be 15% of system refrigerant charge per year [49].

The indirect emission is calculated [46] by

$$Indirect\ Emission = L \times AEC \times EM + \Sigma(MM \times m) + \Sigma(RM \times mr) + RFM \times C + L \times ALR \times RFM \times C + C \times (1 - EOL) \times RFD \quad (6\text{-}2)$$

where AEC is the Annual Energy Consumption, EM is CO_2 produced/kWh, MM is CO_2 produced/kg of Material, m is the mass of material, RM is the CO_2 production for recycled

material, RFM is the Refrigerant Manufacture emission, and RFD is Refrigerant Disposal emission.

The driving distance of US vehicle per year was assumed to be 22,000 km [50]. And the FTP-75 driving cycle was used to calculate the driving time. The life time of the vehicle is assumed to be 9 years[51]. Temperature bin method was used to calculate the annual consumption of MAC. To evaluate the LCCP of DX and SL system in different temperature zones, four cities were selected: Miami, Baltimore, Boston, and Chicago. The weather data were obtained from the third collection of Typical Meteorological Year (TMY3) data base.

Table 6-1: Percentage of Drive Time in Ambient during 6 am to 12 am

T_{amb}[°C]	Chicago	Boston	Baltimore	Miami
<=0	22.73%	14.90%	11.19%	0.00%
0~10	31.49%	32.10%	25.34%	0.35%
10~20	24.93%	30.57%	30.27%	12.91%
20~30	19.37%	21.14%	29.34%	77.53%
30~40	1.49%	1.30%	3.86%	9.21%
>=40	0.00%	0.00%	0.00%	0.00%

The representative temperature for each temperature bin was calculated by summing the hourly temperature within each temperature bin and then divide it by the total number of hours where the temperature is within the boundaries.

The MAC was assumed to be turned on when the ambient temperature is higher than 15°C. The thermal load was calculated by using cabin model developed in Dymola.

The Part Load Factor (PLF) was calculated by [52]

$$PLF = 1 - 0.25 \times (1 - CLF) \tag{6-3}$$

where CLF is the cooling load factor.

Because the electric compressor is used in both air conditioning systems, the compressor RPM is no longer affected by the driving cycle. Therefore, the compressor power consumption was assumed to be constant during the whole process to simplify the calculation. The annual energy consumption is then calculated by

$$AEC = W_{comp}/\eta_{battery} \tag{6-4}$$

where $\eta_{battery}$ is the battery efficiency which is assumed to be 85% for Li-on battery [53]. And the CO_2 emission associate energy input is 0.788 kg CO_2/kWh [54].

The main components in MAC like heat exchangers are mainly built by aluminum, and its manufacturing emission is the highest among other materials [49]. Therefore, only the emission of aluminum production was considered to simplify the calculation.

The refrigerants manufacture emissions can be found on the IIR guideline for LCCP [48,49]. The emissions for R-134a, R-152a and R-1234yf are 8 kg CO_2/kg, 2.2 kg CO_2/kg, and 13.7 kg CO_2/kg. And because the emission during unit disposal takes an only small portion of the LCCP, especially for those refrigerants with low GWP, it can be neglected in the LCCP calculation [49].

The comparison of LCCP of DX and SL system at different locations are displayed in Figure 6-1. As expected, the LCCP increased as the ambient temperature increased, which was a result of high energy consumption caused by the high compressor on time. For system comparison, the direct emission of R-134a DX was 846 kg CO_2, while the direct emission of R-152a SL and R-134a SL were 44 kg CO_2 and 3 kg CO_2, which could be neglected.

Also, it was observed that for cities in cold regions, the LCCP of SL system tends to be lower than that of DX system. While for cities in hot regions like Miami, the LCCP of SL system becomes higher than that of DX system.

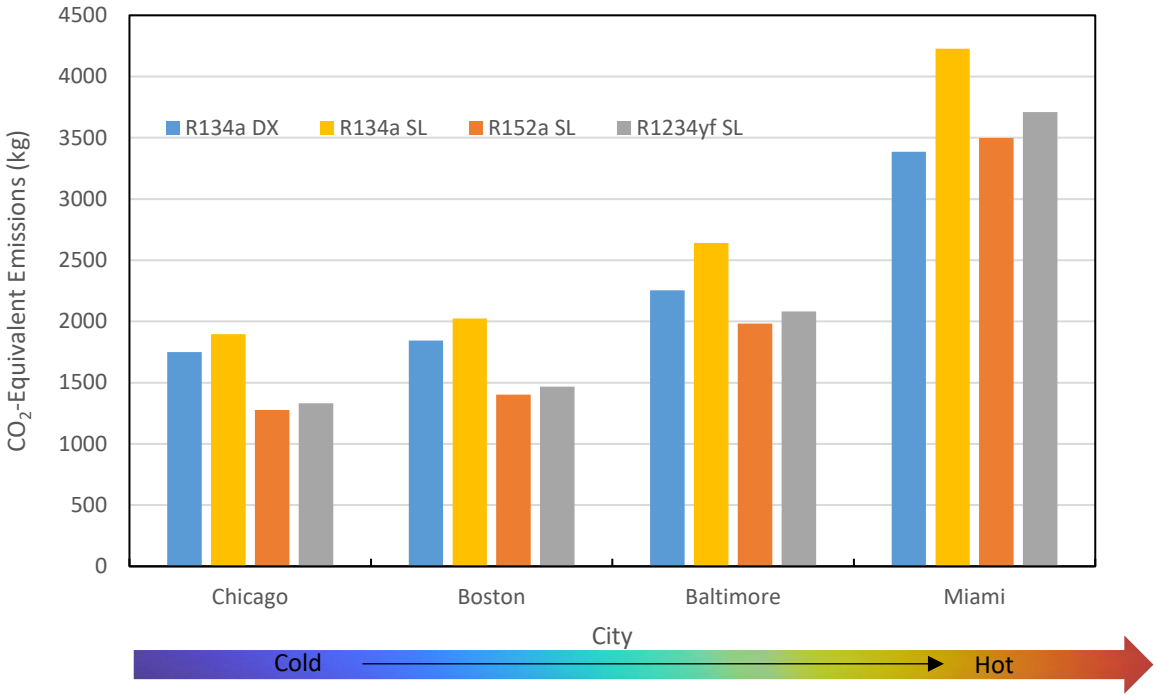

Figure 6-1: LCCP Comparison

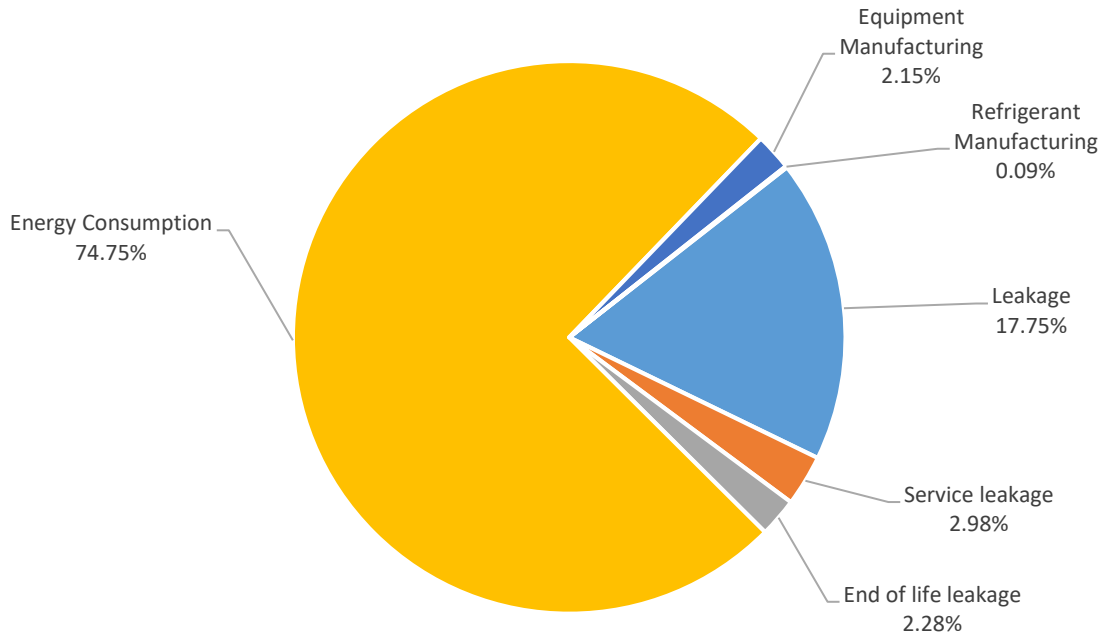

Figure 6-2: R-134a SL LCCP (Baltimore) Breakdown

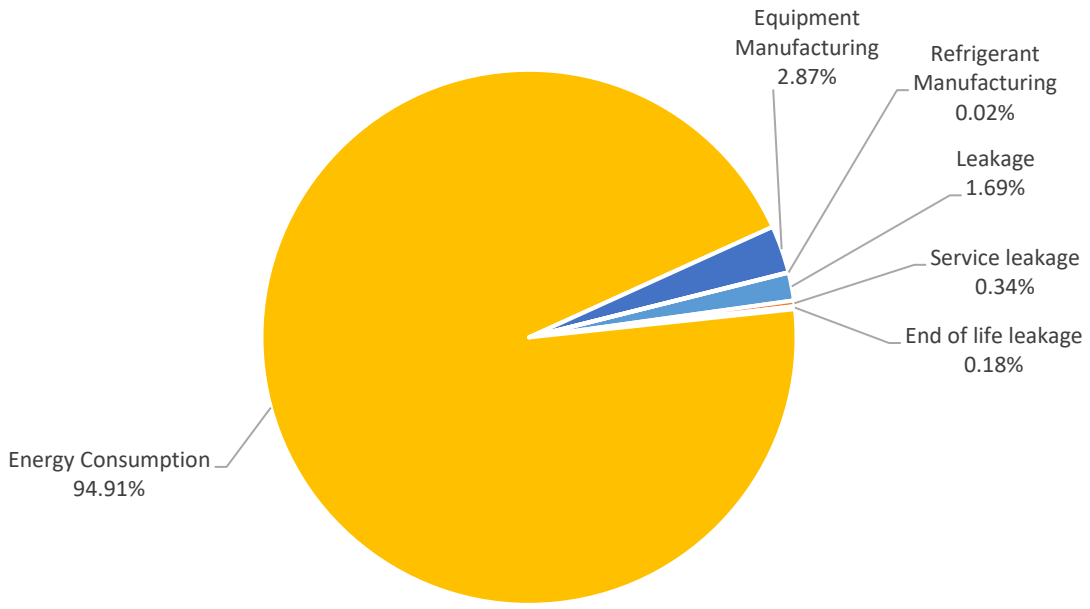

Figure 6-3: R-152a SL LCCP (Baltimore) Breakdown

From Figure 6-2 and Figure 6-3, it was observed that the emissions of energy consumption took accounts for 75% of the total emission of R-134a SL system and 95% of R-152a SL system. This indicated that most emission during the MAC lifetime comes from the energy consumption.

As discussed before, the COP of R-152a SL system was 26 % lower than that of R-134a DX system, meaning that the SL system requires more energy to provide the same amount of cooling.

Therefore, as the ambient temperature increases, the emission of energy consumption of SL system increases much faster than that of DX system. Eventually, for a city like Miami, the additional emission caused by low efficiency cannot be compensated by the reduction in direct emission and the LCCP of SL system becomes higher than the LCCP of DX system. Overall, the SL system is good for application in cold regions. While for cars in the hot region, the DX system has a lower emission.

7 Conclusions

A mobile air conditioning system has secondary loops on both condenser and evaporator sides was proposed. This designed has several advantages. First of all, the evaporator side secondary loop isolates the refrigerant from cabin, which provides safe environment for passengers. Moreover, the introduction of the secondary loops can help reduce the refrigerant charge of system, which leads to low direct green gas emission and low risk of leakage in small incidents. Although the condenser side secondary loop has no positive effect on the system performance during cooling, it provides more heating options for future development, especially for application on electric vehicle.

To compare the performance of the SL system to the DX system, steady-state models for DX system and SL system were developed in EES. The baseline DX system used R-134a as the refrigerant and ethylene glycol-water mixture with 50 wt.% as the coolant for desuperheater. The steady-state and transient models of DX system were validated by the experimental data. The deviation of the evaporator capacity was less than 2% for both steady-state and transient models.

The SL system used R-134a, R-152a, and R-1234yf as its refrigerant and ethylene glycol-water mixture with 50 wt.% as its secondary fluid. The performances of these three refrigerants were compared. R-152a has the best performance in terms of COP, which is 8.9% higher than that of R-134a SL system, the COP of R-1234yf SL system is 2.6% lower than that of R-134a SL system. While the cooling capacity of DX system and SL system are similar, the large COP reduction was observed for SL system. The COP reduction was at least 26.9%. This is mainly due to large compressor work caused by lower suction density and high-pressure ratio. Moreover, the SL system demonstrates large charge reduction when compared to DX system. The refrigerant charge of R-134 DX system is 497 g. While the refrigerant charges for R-134a

SL, R-152a SL, and R-1234yf SL are 239 g, 188 g, and 281 g, respectively. Since the pipe length of the system is unknown, the refrigerant charge inside the pipe is not considered yet. In the real case, the refrigerant charge reduction for SL system should be even better due to short refrigerant pipe length.

In addition to the steady-state performance comparison, the transient performance of SL system was evaluated under the US06 driving cycle. Since in the SL system, the condenser is water-cooled and is not directly cooled by the air, less capacity fluctuation was observed. And all four models showed a relatively stable curve for evaporator capacity. Since in DX system the evaporator is directly used to cool the air, the air temperature inside the cabin drops faster in the beginning.

Moreover, the performances of both DX system and SL system during start/stop operation were evaluated. The results show that both cooling capacity and compressor power consumption decreased of DX and SL systems. And the DX system shows large fluctuation in temperature, which has a negative effect on passenger's thermal comfort. The start/stop operation can increase the COP of R-152a SL by 3.5%, while it will reduce the COP of R-1234yf SL by 2.2%.

To investigate the global warming impact of both DX and SL system, the LCCP of both system using different refrigerant was calculated in four different cities: Chicago, Boston, Baltimore and Miami. The results showed that due to high energy consumption of the SL system, the LCCP of SL system is lower than that of DX system only in cold regions. And R-152a SL has lowest LCCP among three refrigerant in SL system. While R-134a SL has highest LCCP.

The main contribution of this research are listed below:

- Comprehensive steady-state and transient models were developed for both DX and SL systems.
- The steady-state and transient models for DX system using R-134a were validated against the steady-state test results.
- The performances of R-134a, R-152a, and R-1234yf in SL system were compared and discussed.
- Transient simulations were performed under US06 driving condition. Also, system performance when using start/stop operation was evaluated.
- The LCCPs of both DX and SL systems were investigated.

8 Future Work

The steady-state model used in current research has long convergence time. And the current approach by using procedure command in EES doesn't take advantage of the advanced solver of the EES. Therefore, a more advanced approach should be taken to improve the computational efficiency of the steady-state model.

For the transient model, finite volume method was used to simulate the heat exchanger and the moving boundary method has not been implemented. In the future, the heat exchanger model using moving boundary method could be developed and compared to the model using finite volume method to see which model is best.

In addition, current work focuses on the simulation of the SL system. To validate the simulation results, both steady-state and transient experiments of the SL system are of great importance.

Last but not the least, the current SL system has lower COP compared to the conventional DX system. Therefore, methods need to be taken to improve the COP of SL system. For example, one approach could be replacing current heat exchangers with a heat exchanger that has higher heat transfer coefficient. Another approach is to add internal heat exchanger into the SL system. The internal heat exchanger can be used to increase condenser subcooling, which lowers the evaporator inlet superheat. Therefore, the evaporator capacity may be increased. However, adding internal heat exchanger will increase the suction temperature, which means that the suction density will be lower. Therefore, the benefit from the larger condenser subcooling may be offset by the lower refrigerant mass flow rate. Therefore, the effect of adding internal heat exchanger needs to be investigated in the future research.

Bibliography

[1] Contribution of Working Group I to the Fourth Assessment Report of the Intergovernmental Panel on Climate Change, 2007, (n.d.). https://www.ipcc.ch/publications_and_data/ar4/wg1/en/contents.html (accessed July 29, 2017).

[2] DIRECTIVE 2006/40/EC OF THE EUROPEAN PARLIAMENT AND OF THE COUNCIL of 17 May 2006, (n.d.). http://eur-lex.europa.eu/legal-content/EN/TXT/HTML/?uri=CELEX:32006L0040&from=EN (accessed July 11, 2017).

[3] R1234yf Refrigerant, (n.d.). http://www.aa1car.com/library/hfo-1234yf.htm (accessed April 2, 2017).

[4] G.L. Davis, T.C. Scott, Component, Modeling Requirements for Refrigeration System Simulation, in: Purdue University, West Lafayette, IN, 1976. http://docs.lib.purdue.edu/cgi/viewcontent.cgi?article=1220&context=icec (accessed April 1, 2017).

[5] N. Agrawal, S. Bhattacharyya, J. Sarkar, Optimization of two-stage transcritical carbon dioxide heat pump cycles, Int. J. Therm. Sci. 46 (2007) 180–187. doi:10.1016/j.ijthermalsci.2006.04.011.

[6] D.H. Richardson, H. Jiang, D. Lindsay, R. Radermacher, Optimization of vapor compression systems via simulation, (2002). http://docs.lib.purdue.edu/cgi/viewcontent.cgi?article=1528&context=iracc (accessed April 1, 2017).

[7] J. Sarkar, S. Bhattacharyya, M.R. Gopal, Simulation of a transcritical CO2 heat pump cycle for simultaneous cooling and heating applications, Int. J. Refrig. 29 (2006) 735–743. doi:10.1016/j.ijrefrig.2005.12.006.

[8] J.M.S. Jabardo, W.G. Mamani, M.R. Ianella, Modeling and experimental evaluation of an automotive air conditioning system with a variable capacity compressor, Int. J. Refrig. 25 (2002) 1157–1172. doi:10.1016/S0140-7007(02)00002-6.

[9] G.H. Lee, J.Y. Yoo, Performance analysis and simulation of automobile air conditioning system, Int. J. Refrig. 23 (2000) 243–254. doi:10.1016/S0140-7007(99)00047-X.

[10] M. Hosoz, H.M. Ertunc, Artificial neural network analysis of an automobile air conditioning system, Energy Convers. Manag. 47 (2006) 1574–1587. doi:10.1016/j.enconman.2005.08.008.

[11] T.J. Hendricks, Optimization of vehicle air conditioning systems using transient air conditioning performance analysis, SAE Technical Paper, 2001. http://papers.sae.org/2001-01-1734/ (accessed March 19, 2017).

[12] R. Kossel, N.C. Strupp, W. Tegethoff, Effects of Tool Coupling on Transient Simulation of a Mobile Air-Conditioning Cycle, in: 2009: pp. 318–325. doi:10.3384/ecp09430064.

[13] C.S. Junior, N.C. Strupp, N.C. Lemke, J. Koehler, Modeling a Thermoelectric HVAC System for Automobiles, J. Electron. Mater. 38 (2009) 1093–1097. doi:10.1007/s11664-009-0749-8.

[14] J. Ling, M. Eisele, H. Qiao, V. Aute, Y. Hwang, R. Radermacher, Transient Modeling and Validation of an Automotive Secondary Loop Air-Conditioning System, in: 2014. doi:10.4271/2014-01-0647.

[15] K. Wang, M. Eisele, Y. Hwang, R. Radermacher, Review of secondary loop refrigeration systems, Int. J. Refrig. 33 (2010) 212–234. doi:10.1016/j.ijrefrig.2009.09.018.

[16] R. Cabello, D. Sánchez, R. Llopis, J. Catalán, L. Nebot-Andrés, E. Torrella, Energy evaluation of R152a as drop in replacement for R134a in cascade refrigeration plants, Appl. Therm. Eng. 110 (2017) 972–984. doi:10.1016/j.applthermaleng.2016.09.010.

[17] R. Cabello, D. Sánchez, R. Llopis, I. Arauzo, E. Torrella, Experimental comparison between R152a and R134a working in a refrigeration facility equipped with a hermetic compressor, Int. J. Refrig. 60 (2015) 92–105. doi:10.1016/j.ijrefrig.2015.06.021.

[18] G. Li, M. Eisele, H. Lee, Y. Hwang, R. Radermacher, Experimental investigation of energy and exergy performance of secondary loop automotive air-conditioning systems using low-GWP (global warming potential) refrigerants, Energy. 68 (2014) 819–831. doi:10.1016/j.energy.2014.01.018.

[19] S. Daviran, A. Kasaeian, S. Golzari, O. Mahian, S. Nasirivatan, S. Wongwises, A comparative study on the performance of HFO-1234yf and HFC-134a as an alternative in automotive air conditioning systems, Appl. Therm. Eng. 110 (2017) 1091–1100. doi:10.1016/j.applthermaleng.2016.09.034.

[20] J. Navarro-Esbrí, J.M. Mendoza-Miranda, A. Mota-Babiloni, A. Barragán-Cervera, J.M. Belman-Flores, Experimental analysis of R1234yf as a drop-in replacement for R134a in a vapor compression system, Int. J. Refrig. 36 (2013) 870–880. doi:10.1016/j.ijrefrig.2012.12.014.

[21] Y. Zhao, Z. Qi, J. Chen, B. Xu, B. He, Experimental analysis of the low-GWP refrigerant R1234yf as a drop-in replacement for R134a in a typical mobile air conditioning system,

Proc. Inst. Mech. Eng. Part C J. Mech. Eng. Sci. 226 (2012) 2713–2725. doi:10.1177/0954406211435583.

[22] C.-C. Wang, System performance of R-1234yf refrigerant in air-conditioning and heat pump system – An overview of current status, Appl. Therm. Eng. 73 (2014) 1412–1420. doi:10.1016/j.applthermaleng.2014.08.012.

[23] D. Sánchez, R. Cabello, R. Llopis, I. Arauzo, J. Catalán-Gil, E. Torrella, Energy performance evaluation of R1234yf, R1234ze(E), R600a, R290 and R152a as low-GWP R134a alternatives, Int. J. Refrig. 74 (2017) 269–282. doi:10.1016/j.ijrefrig.2016.09.020.

[24] P. Ortega Sotomayor, J.A.R. Parise, Characterization and simulation of an open piston compressor for application on automotive air-conditioning systems operating with R134a, R1234yf and R290, Int. J. Refrig. 61 (2016) 100–116. doi:10.1016/j.ijrefrig.2015.09.004.

[25] M. Ghodbane, An investigation of R152a and hydrocarbon refrigerants in mobile air conditioning, SAE Technical Paper, 1999.

[26] M. Ghodbane, T.D. Craig, J.A. Baker, Demonstration of an energy-efficient secondary loop HFC-152a mobile air conditioning system, Final Rep. US Environ. Prot. Agency. (2007). http://citeseerx.ist.psu.edu/viewdoc/download?doi=10.1.1.233.2430&rep=rep1&type=pdf (accessed March 20, 2017).

[27] M. Eisele, Transient performance evaluation of automotive secondary loop systems, 2012. http://drum.lib.umd.edu/handle/1903/13521 (accessed April 7, 2017).

[28] L. Dentis, A. Mannoni, M. Parrino, HC refrigerants: an ecological solution for automotive a/c systems, in: Veh. Therm. Manag. Syst. Conf. Proc. Lond. UK, 1999: pp. 133–147.

[29] C. Malvicino, S. Riccardo, Thermal Systems Integration for Fuel Economy - TIFFE, in: Adv. Microsyst. Automot. Appl. 2010, Springer, Berlin, Heidelberg, 2010: pp. 109–119. doi:10.1007/978-3-642-16362-3_12.

[30] P.G. ROUSSEAU, G.P. GREYVENSTEIN, M. VAN ELDIK, Detailed Simulation of Fluted Tube Water Heating Condensers.pdf, in: 2000.

[31] J.A. Arnold, S. Garimella, R.N. Christensen, Fluted Tube Heat Exchanger Design Manual, GRI Report 5092–243–2357, 1993.

[32] R.M. Manglik, A.E. Bergles, Heat transfer and pressure drop correlations for the rectangular offset strip fin compact heat exchanger, Exp. Therm. Fluid Sci. 10 (1995) 171–180. doi:10.1016/0894-1777(94)00096-Q.

[33] K. Nishikawa, Y. Fujita, H. Ohta, S. Hidaka, Effect of the surface roughness on the nucleate boiling heat transfer over the wide range of pressure, in: Proc. Seventh Int. Heat Transf. Conf., 1982: pp. 61–66.

[34] D.L. Bennett, M.W. Davis, B.L. Hertzler, Suppression of saturated nucleate boiling by forced convective flow, in: AIChE Symp. Ser., 1980.

[35] B. Kim, B. Sohn, An experimental study of flow boiling in a rectangular channel with offset strip fins, Int. J. Heat Fluid Flow. 27 (2006) 514–521. doi:10.1016/j.ijheatfluidflow.2005.11.008.

[36] R.L. Amalfi, F. Vakili-Farahani, J.R. Thome, Flow boiling and frictional pressure gradients in plate heat exchangers. Part 2: Comparison of literature methods to database and new prediction methods, Int. J. Refrig. 61 (2016) 185–203. doi:10.1016/j.ijrefrig.2015.07.009.

[37] Yi-Yie Yan, Hsiang-Chao Lio, Tsing-Fa Li, Condensation heat transfer and pressure drop of refrigerantR134aa in a plate heat exchanger.pdf, Int. J. Heat Mass Transf. 42 (1998) 993–1006.

[38] R.W. Lockhart, R.C. Martinelli, Proposed correlation of data for isothermal two-phase, two-component flow in pipes, Chem Eng Prog. 45 (1949) 39–48.

[39] D.E. Metzger, W.B. Shepard, S.W. Haley, Row Resolved Heat Transfer Variations in Pin-Fin Arrays Including Effects of Non-Uniform Arrays and Flow Convergence, (1986) V004T09A015. doi:10.1115/86-GT-132.

[40] T.L. Bergman, F.P. Incropera, eds., Fundamentals of heat and mass transfer, 7th ed, Wiley, Hoboken, NJ, 2011.

[41] R. Yun, J. Hyeok Heo, Y. Kim, Evaporative heat transfer and pressure drop of R410A in microchannels, Int. J. Refrig. 29 (2006) 92–100. doi:10.1016/j.ijrefrig.2005.08.005.

[42] M.M. Shah, A general correlation for heat transfer during film condensation inside pipes, Int. J. Heat Mass Transf. 22 (1979) 547–556.

[43] Yujuei Chang, Chichuan Wang, A generalized heat transfer correlation for louver fin.pdf, Int J Heat Mass Transf. 40 (1997) 533–544.

[44] C.-C.D. Huang, A dynamic computer simulation model for automobile passenger compartment climate control and evaluation, 1998.

[45] O. US EPA, Dynamometer Drive Schedules, US EPA. (2015). https://www.epa.gov/vehicle-and-fuel-emissions-testing/dynamometer-drive-schedules (accessed July 12, 2017).

[46] S. Troch, H. Lee, Y. Hwang, R. Radermacher, Harmonization of Life Cycle Climate Performance (LCCP) Methodology, (2016). http://docs.lib.purdue.edu/iracc/1724/ (accessed July 14, 2017).

[47] W. Schwarz, J. Harnisch, Establishing the leakage rates of mobile air conditioners, Rep. Prep. DG Environ. Eur. Comm. Ecofys Öko-Rech. Ecofys Frankf. Ger. (2003). http://www.oekorecherche.de/sites/default/files/publikationen/leakage_rates_0.pdf (accessed July 13, 2017).

[48] S. Papasavva, W.R. Hill, S.O. Andersen, GREEN-MAC-LCCP: A Tool for Assessing the Life Cycle Climate Performance of MAC Systems, Environ. Sci. Technol. 44 (2010) 7666–7672. doi:10.1021/es100849g.

[49] Life Cycle Climate Performance Working Group, Guideline for Life Cycle Climate Performance, 2015. http://www.iifiir.org/userfiles/file/about_iir/working_parties/WP_LCCP/07/LCCP-WP_Booklet-LCCP-Guideline-V7_2015-08.pdf (accessed July 12, 2017).

[50] A. Hafner, P. Neks\a a, J. Pettersen, Life Cycle Climate Performance (LCCP) of mobile air-conditioning systems with HFC-134a, HFC-152a and R-744, Proc. Mob. Air Cond. Summit. 15 (2004). http://www.centrogalileo.it/NUOVAPA/Articoli%20tecnici/INGLESE%20CONVEGNO/CO2/Neksa%20-%20SINTEF_LCCP_MAC_CO2.pdf (accessed April 7, 2017).

[51] S. Papasavva, GREEN-MAC-LCCP, (2007). http://www.sae.org/events/aars/presentations/2007papasavva.pdf (accessed July 24, 2017).

[52] S. Katipamula, D.L. O'Neal, A part load factor for a heat pump derived from laboratory measurements, Energy Build. 19 (1992) 125–132. doi:10.1016/0378-7788(92)90006-3.

[53] L.O. Valøen, M.I. Shoesmith, The effect of PHEV and HEV duty cycles on battery and battery pack performance, in: PHEV 2007 Conf., 2007: pp. 4–5. http://www.umanitoba.ca/outreach/conferences/phev2007/PHEV2007/proceedings/PluginHwy_PHEV2007_PaperReviewed_Valoen.pdf (accessed August 7, 2017).

[54] S. Troch, HARMONIZATION OF LIFE CYCLE CLIMATE PERFORMANCE AND ITS IMPROVEMENT FOR HEAT PUMP APPLICATIONS, 2016. http://drum.lib.umd.edu/bitstream/handle/1903/18386/Troch_umd_0117N_17141.pdf?sequence=1&isAllowed=y (accessed August 7, 2017).